PHYSICAL REVIEW D **88,** 103509 (2013)

Dynamical Dark Matter and the positron excess in light of AMS results

Keith R. Dienes,[1,2,3,*] Jason Kumar,[4,†] and Brooks Thomas[4,‡]

[1]*Physics Division, National Science Foundation, Arlington, Virginia 22230, USA*
[2]*Department of Physics, University of Maryland, College Park, Maryland 20742, USA*
[3]*Department of Physics, University of Arizona, Tucson, Arizona 85721, USA*
[4]*Department of Physics, University of Hawaii, Honolulu, Hawaii 96822, USA*

(Received 8 July 2013; revised manuscript received 16 October 2013; published 8 November 2013)

The AMS-02 experiment has recently released data which confirms a rise in the cosmic-ray positron fraction as a function of energy up to approximately 350 GeV. Over the past decade, attempts to interpret this positron excess in terms of dark-matter decays have become increasingly complex and have led to a number of general expectations about the decaying dark-matter particles: such particles cannot undergo simple two-body decays to leptons, for example, and they must have rather heavy TeV-scale masses. In this paper, by contrast, we show that Dynamical Dark Matter can not only match existing AMS-02 data on the positron excess, but also accomplish this feat with significantly lighter dark-matter constituents undergoing simple two-body decays to leptons. Moreover, we demonstrate that this can be done without running afoul of numerous other competing constraints from FERMI and Planck on decaying dark matter. Finally, we demonstrate that the Dynamical Dark Matter framework makes a fairly robust prediction that the positron fraction should level off and then remain roughly constant out to approximately 1 TeV, without experiencing any sharp downturns. Indeed, if we interpret the positron excess in terms of decaying dark matter, we find that the existence of a plateau in the positron fraction at energies less than 1 TeV may be taken as a ''smoking gun'' of Dynamical Dark Matter.

DOI: 10.1103/PhysRevD.88.103509 PACS numbers: 95.35.+d, 98.80.Cq, 14.80.Rt, 11.25.Wx

I. INTRODUCTION

One of the most urgent problems facing particle physics, astrophysics, and cosmology today is that of understanding the nature of dark matter. Fortunately, a confluence of emerging data from direct-detection, indirect-detection, and collider experiments suggests that major progress may soon be at hand. A potentially important ingredient in this mix may involve recent results [1] from the AMS-02 experiment on the flux of cosmic-ray positrons at energies up to 350 GeV. These results confirm the anomalous and puzzling results observed by earlier cosmic-ray detectors such as HEAT [2], AMS-01 [3,4], PAMELA [5,6], and FERMI [7] which indicate that the positron fraction—i.e., the ratio of the differential flux Φ_{e^+} of cosmic-ray positrons to the combined differential flux $\Phi_{e^-} + \Phi_{e^+}$ of cosmic-ray electrons and positrons—actually rises as a function of particle energy E_e for energies $E_e \gtrsim 10$ GeV. Since the positron fraction is generally expected to fall with energy in this energy range, the observed positron excess suggests that some unanticipated physics might be in play. While many possibilities exist, one natural idea is that these positrons may be produced via the annihilation or decay of dark-matter particles within the galactic halo. Unfortunately, this rise in the positron flux occurs without any other distinctive features, and no downturn at high energies—a standard prediction of the most straightforward dark-matter models—is apparent. This rise in the positron fraction therefore poses a major challenge for any potential interpretation in terms of dark-matter physics.

At first glance, it might seem relatively straightforward to interpret the observed positron excess in terms of annihilating or decaying dark-matter particles within the galactic halo. However, such a dark-matter interpretation of the cosmic-ray positron excess is tightly constrained by a number of additional considerations. For example, no corresponding excess is observed in the flux of cosmic-ray antiprotons [8], a fact which significantly constrains the particle-physics properties of possible dark-matter candidates. Indeed, these constraints are particularly severe for dark-matter candidates which annihilate or decay either predominately to strongly interacting Standard-Model (SM) particles or to particles such as $W^{\pm}$ or Z whose subsequent decays produce such particles with significant frequency. For this reason, the most natural dark-matter candidates which can explain the observed positron excess are those which annihilate or decay primarily to charged leptons.

However, even such ''leptophilic'' dark-matter candidates are significantly constrained by cosmic-ray data. Precise measurements of the combined-flux spectrum of cosmic-ray electrons and positrons by the FERMI Collaboration [9] further restrict the range of viable dark-matter models of the observed positron excess. Moreover, constraints on the production of photons are also quite stringent. For example, high-energy photons produced by a cosmological population of dark-matter particles contribute to the diffuse

*dienes@physics.arizona.edu
†jkumar@phys.hawaii.edu
‡thomasbd@phys.hawaii.edu

extragalactic gamma-ray background which has been measured by the FERMI Collaboration [10]. In addition, the energy released via the annihilation or decay of dark-matter particles in the early universe can also lead to a reionization of the thermal plasma at or after the time of last scattering. This in turn induces a modification of the observed temperature and polarization fluctuations of the cosmic microwave background (CMB). As a result, CMB data from BOOMERANG [11], ACBAR [12], WMAP [13], and Planck [14] significantly constrain the rate at which dark matter can annihilate or decay during and after the recombination epoch.

A number of scenarios have been advanced over the past decade to reconcile the observed positron fraction with these additional constraints [15]. As these constraints have sharpened over time, the corresponding dark-matter models have also grown in complexity and sophistication—a trend which has only continued [16] since the release of the most recent AMS-02 data. For example, one current possibility [17] involves a dark-matter particle which annihilates or decays into exotic intermediate states which only subsequently decay into $\mu^{\pm}$ or $\pi^{\pm}$. Other possibilities [18,19] involve dark-matter particles which decay primarily via three-body processes of the form $\chi \to \psi \ell^+ \ell^-$, where ψ is an additional, lighter dark-sector field and where $\ell^{\pm} = \{e^{\pm}, \mu^{\pm}, \tau^{\pm}\}$. There also exist other three-body-decay models [20,21] in which all of the final states are in the visible sector. In each case, these features are required in order to ensure that the resulting electron- and positron-flux spectra are significantly ''softer'' (i.e., broader, more gently sloped) than those produced by a dark-matter particle undergoing a two-body decay directly to SM states. Indeed, only such softer spectra can provide a satisfactory combined fit to the observed positron fraction and to the $\Phi_{e^+} + \Phi_{e^-}$ flux spectrum observed by FERMI while simultaneously satisfying all other phenomenological constraints.

Taken together, these attempts have led to certain expectations concerning the nature of the dark-matter particle whose decays or annihilations might explain the positron excess. Specifically, it is expected that this dark-matter particle will not undergo two-body decays to Standard-Model states, but will instead decay through more complex decay patterns such as those involving nontrivial intermediate states or three-body final states. As discussed above, this is necessary in order to soften the kinematic spectrum associated with such single-particle dark-matter candidates. Second, it is also expected that such dark-matter particles must be relatively heavy, with masses $\sim\mathcal{O}$(TeV), in order to properly explain the measured positron excess. This is unfortunate, since leptophilic particles with such heavy masses are typically difficult to probe via other experiments (e.g., existing collider experiments) which provide complementary probes of the dark sector. Finally, we note that all current dark-matter-based attempts at explaining the observed positron excess inevitably predict that the positron fraction will experience a relatively sharp downturn at energies which do not greatly exceed current sensitivities. Indeed, a relatively sharp downturn is in some sense required by the decay kinematics of such dark-matter candidates.

In this paper, we will show that Dynamical Dark Matter (DDM) [22,23] can provide an entirely different perspective on these issues. First, we shall demonstrate that a leptonically decaying DDM ensemble can successfully account for the observed positron excess and combined cosmic-ray $e^{\pm}$ flux without running afoul of any other applicable constraints on decaying or annihilating dark-matter particles. Second, we shall show that DDM can do this entirely with dark-matter components undergoing simple two-body decays to leptons—indeed, more complicated decay phenomenologies are not required. Third, we shall find that the DDM components which play the dominant role in explaining the positron excess are themselves relatively light, with masses only in the $\mathcal{O}$(200–500) GeV range. This is an important distinction relative to more traditional models, opening up the possibility of correlating these positron-flux signatures with possible missing-energy signatures in collider experiments. This would then allow a more tightly constrained, complementary approach to studying such dark-matter candidates. Indeed, as we shall see, DDM accomplishes all of these feats by providing an *alternative* method of softening the flux spectra—not through a complicated set of dark-matter decay/annihilation channels (and thus complicated particle kinematics), but instead through a richer and more complex dark sector itself.

But perhaps most importantly, we shall show that DDM also makes a fairly firm prediction for the positron fraction at energies *beyond* 350 GeV: the positron fraction will level off and remain roughly constant all the way up to energies of approximately 1 TeV. Indeed, as we shall find, this behavior for the positron fraction emerges for most of the viable regions of DDM parameter space. Hence, within such regions, the DDM framework predicts that no abrupt downturn in the positron fraction will be seen. This is a marked difference relative to most traditional dark-matter models which seek to explain the positron excess: indeed, most of these models predict either a continuing rise in the positron fraction or the onset of a downturn, but cannot easily accommodate a relatively flat plateau. Thus, if we interpret the positron excess seen by AMS-02 as resulting from dark-matter annihilations or decays, a relatively flat plateau in the positron fraction at energies less than 1 TeV may be taken as a ''smoking gun'' of Dynamical Dark Matter.

This paper is organized as follows. In Sec. II, we briefly review the general properties of DDM ensembles and introduce the general parametrizations we shall use in order to characterize these ensembles in our analysis. In Sec. III, we then discuss the $e^{\pm}$ injection spectra produced

by the decays of a DDM ensemble and show how these spectra are modified upon propagation through the interstellar medium. In Sec. IV, we then discuss the additional considerations which further constrain decaying dark-matter candidates and examine how these considerations apply to DDM ensembles. Our main results appear in Sec. V, where we demonstrate that DDM ensembles can indeed reproduce the observed positron excess while simultaneously satisfying all relevant constraints—even with relatively light DDM constituents undergoing simple two-body leptonic decays. We also demonstrate that most of the viable DDM parameter space leads to the prediction of a positron fraction which levels off and remains roughly constant out to energies of approximately 1 TeV. Even though (as we shall see) there exist other regions of viable DDM parameter space for which the predicted positron excess can experience a downturn (or even an oscillation) as a function of energy, we shall explain why we nevertheless believe that the existence of a plateau in the positron fraction can serve as a "smoking gun" for the Dynamical Dark Matter framework as a whole. In Sec. VI, we then discuss the extent to which these results continue to apply when our fundamental theoretical assumptions and computational procedures are altered. Finally, in Sec. VII, we conclude with a summary of our results and a discussion of their implications for distinguishing between decaying DDM ensembles and other proposed explanations for the positron excess, including those involving purely traditional astrophysical sources.

II. THE DDM ENSEMBLE: FUNDAMENTAL CHARACTERISTICS

Dynamical Dark Matter [22,23] is an alternative framework for dark-matter physics in which the requirement of dark-matter stability is replaced by a balancing of lifetimes against cosmological abundances across an ensemble of individual dark-matter components with different masses, lifetimes, and abundances. It is this DDM ensemble which collectively serves as the dark-matter "candidate" in the DDM framework, and which collectively carries the observed dark-matter abundance $\Omega_{\rm CDM}$. Likewise, it is the balancing between lifetimes and abundances across the ensemble as a whole which ensures the phenomenological viability of the DDM framework [23,24]. In some sense the DDM ensemble is the most general dark sector that can be envisioned, reducing to a standard stable dark-matter candidate in the limit that the number of dark-matter components is taken to one. However, in all other cases, stability is not an absolute requirement in the DDM framework (a feature which distinguishes DDM from other multicomponent dark-matter scenarios), but instead depends, component by component, on the corresponding cosmological abundances. As has been discussed in Refs. [22,23,25], DDM ensembles appear naturally in many extensions to the Standard Model, including string theory and theories with large extra spacetime dimensions, and not only possess a highly nontrivial cosmology but can also lead to many striking signatures at colliders [25] and direct-detection experiments [26]—signatures which transcend those associated with traditional dark-matter candidates. Indeed, DDM ensembles are fairly ubiquitous, and can also potentially arise in a variety of additional contexts ranging from theories such as the axiverse [27] to theories involving large hidden-sector gauge groups and even theories exhibiting warped stringy throats [28].

It is the purpose of this paper to examine the behavior of the positron flux within the context of the general DDM framework, and thereby study the implications of the DDM framework for *indirect*-detection experiments. Because the DDM framework lacks dark-matter stability as a founding principle, discussions of decaying dark matter (such as those possibly leading to a cosmic-ray positron excess) are particularly relevant for DDM. Indeed, one important characteristic of DDM is that the DDM dark sector includes particles whose lifetimes can in principle collectively span a vast range of time scales from well before to long after the present day. Understanding the impacts of such decays for present-day cosmic-ray physics is therefore of paramount importance.

Because our goal in this paper is to explore the cosmic-ray phenomenology to which DDM ensembles can give rise, we shall avoid focusing on a specific DDM model and instead assume a general ensemble configuration of individual dark-matter components ϕ_n whose masses m_n are given by a relation of the form

$$m_n = m_0 + n^\delta \Delta m, \tag{2.1}$$

where the mass splitting Δm and scaling exponent δ are both assumed positive. Thus the index $n = 0, 1, 2, \ldots$ labels the ensemble constituents in order of increasing mass. Likewise, we shall assume that these components ϕ_n have cosmological abundances Ω_n and decay widths Γ_n which can be parametrized according to general scaling relations of the form

$$\Omega_n = \Omega_0 \left(\frac{m_n}{m_0}\right)^\alpha, \qquad \Gamma_n = \Gamma_0 \left(\frac{m_n}{m_0}\right)^\gamma \tag{2.2}$$

where α and γ are general power-law exponents. While the existence of such scaling relations is not a fundamental requirement of the DDM framework, relations such as these do arise naturally in a number of explicit realistic DDM models [22,23,25] and allow us to encapsulate the structure of an entire DDM ensemble in terms of only a few well-motivated parameters. Note that the decay width Γ_n in Eq. (2.2) refers to (or is otherwise assumed to be dominated by) the decay of ϕ_n to SM states, and likewise Ω_n denotes the cosmological abundance that ϕ_n *would have had* at the present time if it had been absolutely stable. Indeed, because the DDM framework allows each individual ϕ_n component to decay at a different time, the corresponding

abundances Ω_n generally evolve in a nontrivial manner across the DDM ensemble [22], and thus no single scaling relation can hold across the ensemble for all times.

Given these scaling relations, our DDM ensemble is in principle described by the seven parameters $\{\alpha, \gamma, \delta, m_0, \Omega_0, \Gamma_0, \Delta m\}$. For convenience, in this paper we shall fix $\delta = 1$ and $\Delta m = 1$ GeV; these choices ensure that our DDM ensemble transcends a mere set of individual dark-matter components and observationally acts as a "continuum" of states relative to the scale set by the energy resolution of the relevant cosmic-ray detectors. We shall also fix Ω_0 by requiring that the ensemble carry the entire observed dark-matter abundance $\Omega_{\rm CDM}$; this will be discussed further below. Of the remaining four parameters, we shall treat $\{\alpha, \gamma, m_0\}$ as free parameters and eventually survey over different possibilities within the ranges $-3 \leq \alpha < 0$, $-1 \leq \gamma \leq 2.5$, and 100 GeV $\lesssim m_0 \lesssim 1$ TeV. Given a specific assumption for how each ϕ_n decays to Standard-Model states, we will then find that each such choice of $\{\alpha, \gamma, m_0\}$ leads to a unique prediction for the overall shape of the resulting electron and positron fluxes as functions of energy, with an arbitrary normalization set by the lifetime $\tau_0 \equiv 1/\Gamma_0$ of the lightest dark-matter component in the ensemble. For each choice of $\{\alpha, \gamma, m_0\}$, the final remaining parameter τ_0 can therefore be determined through a best-fit analysis, and indeed we shall find that most scenarios of interest have $\tau_0 \gtrsim 10^{26}$ s. Thus, in this paper, the three quantities $\{\alpha, \gamma, m_0\}$ shall serve as our independent degrees of freedom parametrizing our DDM ensemble.

There are also additional phenomenological considerations which can be used to place bounds on these parameters. For example, one generic feature of the DDM framework is an expected balancing of decay widths against abundances across the DDM ensemble. This expectation comes from the general observation that the earlier a dark-matter component might decay during the evolution of the universe, the smaller its cosmological abundance must be in order to avoid the disruptive effects of that decay and remain phenomenologically viable [22–24]. We therefore expect to find, roughly speaking, an *inverse* relation between cosmological abundances and decay widths, or equivalently that $\alpha\gamma < 0$. Indeed, as indicated above, it is usually α which will be negative in most DDM scenarios, while γ is generally positive. However, for illustrative purposes, in this paper we shall also occasionally consider extrapolations into regions of parameter space with $\alpha\gamma > 0$.

Likewise, in this paper we also shall focus on regions of parameter space in which γ is not too large. Our reasons, again, are primarily phenomenological. In general, our interest in this paper concerns the contributions that the dark-matter components ϕ_n might, through their decays, make to the differential electron/positron fluxes $\Phi_{e^\pm}$ within the energy range 20 GeV $\lesssim E_{e^\pm} \lesssim 1$ TeV. One of the most interesting regions of parameter space will therefore be that in which all of the ϕ_n which could in principle yield a non-negligible contribution to these fluxes are sufficiently long-lived that their abundances Ω_n are effectively undiminished by decays and consequently still scale according to Eq. (2.2) at the present time. Indeed, this is the regime within which the full DDM ensemble plays the most significant role in indirect-detection phenomenology and within which the most distinctive signatures arise. In order to specify where this regime lies within the parameter space of our DDM model, we begin by noting that the contribution from extremely heavy dark-matter components ϕ_n to $\Phi_{e^\pm}$ will be comparatively negligible (i.e., below background) for $E_{e^\pm} \lesssim 1$ TeV. We therefore define a fiducial mass scale m_* to represent this cutoff, and demand that all components ϕ_n with masses $m_n < m_*$ have lifetimes $\tau_n > t_{\rm now}$, where $t_{\rm now} \approx 4.3 \times 10^{17}$ s is the age of the universe. The scaling relation for Γ_n in Eq. (2.2) implies that this condition may be written as a constraint on the scaling exponent γ:

$$\gamma \lesssim \frac{\ln(\tau_0/t_{\rm now})}{\ln(m_*/m_0)}. \tag{2.3}$$

For any ensemble with $\tau_0 \gtrsim 10^{26}$ s and $m_0 \gtrsim 200$ GeV, we find that the conservative choice $m_* = 10^6$ GeV yields the limit $\gamma \lesssim 2.26$. As we shall see in Sec. V, it is not difficult to satisfy the condition in Eq. (2.3) while simultaneously reproducing the positron-fraction curve reported by AMS-02 and satisfying all other applicable constraints. However, we hasten to emphasize that the criterion in Eq. (2.3) does *not* represent a parameter-space constraint which our DDM model must satisfy for theoretical or phenomenological consistency. By contrast, it merely defines a regime of particular phenomenological interest within our model.

Finally, in order to evaluate the contribution to the observed cosmic-ray electron and positron fluxes from such a DDM ensemble, it is necessary to specify not only the particle-physics properties of the DDM ensemble itself but also certain astrophysical properties of the ensemble which characterize how the populations of the various ϕ_n are distributed throughout the galactic halo. First, for this analysis, we assume that the DDM ensemble contributes essentially the entirety of the present-day dark-matter abundance, and therefore that the total DDM ensemble abundance

$$\Omega_{\rm tot} \equiv \Omega_0 \sum_{n=0}^{n_{\rm max}} \left(1 + n^\delta \frac{\Delta m}{m_0}\right)^\alpha \tag{2.4}$$

matches the total dark-matter abundance $\Omega_{\rm CDM} h^2 \approx 0.1131 \pm 0.0034$ observed by WMAP [13]. (Although recent Planck results [14] suggest the slightly higher value $\Omega_{\rm CDM} h^2 \approx 0.1199 \pm 0.0027$, such a shift in $\Omega_{\rm CDM}$ has an essentially negligible effect on our results.) Note that since we are considering only those DDM ensembles for which $\alpha\delta < -1$, the sum in Eq. (2.4) remains convergent in the

$n_{\max} \to \infty$ limit [26]. Second, we make the simplifying assumption that the density profiles $\rho_n(r)$ according to which our individual dark-matter components ϕ_n are distributed within the galactic halo share a common functional form, which we model using an NFW profile [29]. Finally, for simplicity, we take the normalization of each $\rho_n(r)$ within the galactic halo—which is typically specified by the local dark-matter density $\rho_n^{\rm loc}$ within the solar neighborhood—to be proportional to the global energy density of the corresponding constituent. Thus, we shall assume that $\rho_n^{\rm loc}/\rho_{\rm tot}^{\rm loc} = \Omega_n/\Omega_{\rm tot}$ in what follows, with $\rho_{\rm tot}^{\rm loc} \approx 0.3\ {\rm GeV/cm^3}$.

III. ELECTRON/POSITRON PRODUCTION AND PROPAGATION

In general, a given dark-matter particle ϕ undergoes a decay of the form $\phi \to f$ where f is a multiparticle final state which includes at least some visible-sector fields. Using only visible-sector physics, one can then extract a set of differential electron and positron fluxes $dN_{f,e^\pm}/dE_{e^\pm}$ which reflect not only the kinematics of how f subsequently decays to electrons and positrons, but also the possible decay chains and branching ratios that might be involved in such subsequent processes, the effects of final-state radiation, and so forth. However, $dN_{f,e^\pm}/dE_{e^\pm}$ only describes the differential fluxes at the location where these electrons and positrons were originally produced (here assumed to be somewhere within our galaxy); it is still necessary to use this so-called "injection" spectrum $dN_{f,e^\pm}/dE_{e^\pm}$ in order to determine the final electron and positron differential fluxes $\Phi_{e^\pm}$ that will emerge and be measured after these particles have propagated through the interstellar medium (ISM) and entered our solar neighborhood. In this section, we shall discuss how these final observed differential fluxes $\Phi_{e^\pm}$ may be determined, focusing on the case when our injection spectrum $dN_{f,e^\pm}/dE_{e^\pm}$ arises from an entire DDM ensemble. Note, in particular, that our interest in this paper centers on the *differential* fluxes $\Phi_{e^\pm}$; these quantities are related to the *total* fluxes $\tilde{\Phi}_{e^\pm}$ via $\Phi_{e^\pm} \equiv d\tilde{\Phi}_{e^\pm}/dE_{e^\pm}$. Indeed, it is only the differential fluxes $\Phi_{e^\pm}$ which exhibit the all-important energy dependence which is ultimately the focus of our analysis. In this vein, we also note that we are only concerned in this paper with total differential fluxes integrated over all angles, and not with their directional dependence.

In general, these differential fluxes $\Phi_{e^\pm}$ can be expressed as

$$\Phi_{e^\pm} = \frac{v}{4\pi} f_{e^\pm}(E) \tag{3.1}$$

where $f_{e^\pm}(E)$ denotes the local differential number density of electrons and positrons per unit energy and where $v \approx c$ denotes the velocity of the incident particles. Taken as a function of position, energy, and time, this number density $f_\pm(E, \vec{r}, t)$ is in turn determined by the transport equation

$$\frac{\partial f_{e^\pm}}{\partial t} = \vec{\nabla} \cdot [K(E, \vec{r}) \vec{\nabla} f_{e^\pm}] + \frac{\partial}{\partial E}[b(E, \vec{r}) f_{e^\pm}] + Q_{e^\pm}(E, \vec{r}, t), \tag{3.2}$$

where $Q_{e^\pm}(E, \vec{r}, t)$ is the source term for electron and positron production, where $K(E, \vec{r})$ is the diffusion coefficient, and where $b(E, \vec{r})$ is the energy-loss rate. For an approximately steady-state process, we may take $Q_{e^\pm}(E, \vec{r}, t) \approx Q_{e^\pm}(E, \vec{r})$ as effectively independent of time, and thus we have $\partial f_{e^\pm}/\partial t = 0$. Of course, the total injection rate $dN_{f,e^\pm}/dE_{e^\pm}$ associated with the decaying constituents of a DDM ensemble will by nature be time dependent. However, for ensembles capable of producing a non-negligible contribution to observed electron and positron fluxes, we shall see that the time scale on which this variation is significant is far greater than the time scale for $e^\pm$ diffusion through the galactic halo. Thus this steady-state approximation is justified.

Following Ref. [30], we next adopt a stationary two-zone diffusion model in which the diffusion coefficient is spatially constant throughout the diffusion zone and takes the form

$$K(E) = \frac{v}{c} K_0 \mathcal{R}^\epsilon, \tag{3.3}$$

where K_0 and ϵ are free parameters which characterize a particular diffusion model and where $\mathcal{R}$ is the so-called "rigidity" of the particle (defined as the ratio of its momentum in GeV to its electromagnetic charge in units of the electron charge e). Note that for electrons and positrons with $E \gg m_e \approx 511$ keV, the diffusion coefficient may also be expressed as $K(E) \approx K_0 (E/{\rm GeV})^\epsilon$. The energy-loss rate $b(E, \vec{r})$ includes contributions from both synchrotron radiation and inverse-Compton scattering and can be written in the form

$$b(E, \vec{r}) = \frac{32\pi\alpha_{\rm EM}^2}{9 m_e^4} E^2 \left[u_B(\vec{r}) + \sum_i u_{\gamma,i}(\vec{r}) R_i^{\rm KN}(E) \right], \tag{3.4}$$

where $u_B(\vec{r})$ is the energy density in galactic magnetic fields; where the $u_{\gamma,i}(\vec{r})$ are the contributions to the photon energy density from the CMB, starlight, and diffuse infrared light ($i = 1, 2, 3$, respectively); and where the functions $R_i^{\rm KN}(E)$ describe the energy dependence of the corresponding contributions from these three sources. The functional forms for $u_B(\vec{r})$, the $u_{\gamma,i}(\vec{r})$, and the $R_i^{\rm KN}(E)$ can be found in Ref. [31] and references therein. Finally, the diffusion zone is assumed to be cylindrical, with a radius R_D and half height L_D. For this analysis we adopt the so-called "MED" propagation model of Refs. [32,33] in which $\epsilon = 0.70$, $\mathcal{K}_0 = 0.0112\ {\rm kpc^2/Myr}$, $L_D = 4$ kpc, and $R_D = 20$ kpc. Other choices will be discussed in Sec. VI.

In general, it is the source terms $Q_{e^\pm}(E, \vec{r})$ which encode the specific dark-matter model under scrutiny and its possible decay patterns. For a DDM model consisting of an ensemble of dark-matter components ϕ_n, the source terms $Q_{e^\pm}(E, \vec{r})$ for electrons and positrons take the general form

$$Q_{e^\pm}(E,\vec{r}) = \sum_{n=0}^{n_{\max}} \frac{\rho_n(\vec{r})}{m_n}\Gamma_n \sum_f \mathrm{BR}(\phi_n \to f)\frac{dN^{(n)}_{f,e^\pm}}{dE_{e^\pm}}, \quad (3.5)$$

where ρ_n denotes the energy density of the DDM component ϕ_n, where $\mathrm{BR}(\phi_n \to f)$ denotes the branching fraction for the decay $\phi_n \to f$, and where $dN^{(n)}_{f,e^\pm}/dE'_{e^\pm}$ are the differential injection spectra produced by each such decay. The solution to Eq. (3.2) can therefore be expressed in the form

$$\begin{aligned}\Phi^{\mathrm{DDM}}_{e^\pm}(E_\pm,\vec{r}) &\approx \frac{c}{4\pi}\sum_{n=0}^{n_{\max}}\frac{\Gamma_n}{m_n}\int d^3\vec{r}\,'\rho_n(\vec{r}\,') \\ &\times \int_0^{m_n/2} dE'_{e^\pm} G_{e^\pm}(E_{e^\pm},E'_{e^\pm};\vec{r},\vec{r}\,') \\ &\times \sum_f \mathrm{BR}(\phi_n\to f)\frac{dN^{(n)}_{f,e^\pm}}{dE'_{e^\pm}}(E'_{e^\pm}),\end{aligned} \quad (3.6)$$

where $G_{e^\pm}(E_{e^\pm},E'_{e^\pm};\vec{r},\vec{r}\,')$ is the Green's function solution to Eq. (3.2). Indeed, this equation indicates that the differential flux which results from the decaying DDM ensemble is nothing but the sum of the individual differential fluxes which would have resulted from the decays of each DDM component individually—precisely as expected for an essentially linear propagation model wherein the Green's function $G_{e^\pm}(E_{e^\pm},E'_{e^\pm};\vec{r},\vec{r}\,')$ encapsulates the essence of propagation through the interstellar medium.

For a DDM ensemble parametrized as in Sec. II—and under the assumption that the galactic energy densities $\rho_n(\vec{r}\,')$ are approximately proportional to the corresponding global energy densities $\rho_n = \Omega_n\rho_{\mathrm{crit}}$—the expression in Eq. (3.6) takes the form

$$\begin{aligned}\Phi^{\mathrm{DDM}}_{e^\pm} &\approx \frac{c\Omega_0}{4\pi\Omega_{\mathrm{tot}}\tau_0 m_0}\sum_{n=0}^{n_{\max}}\left(1+n^\delta\frac{\Delta m}{m_0}\right)^{\alpha+\gamma-1} \\ &\times \int d^3\vec{r}\,'\rho_{\mathrm{tot}}(\vec{r}\,')\int_0^{(m_0+n^\delta\Delta m)/2} dE'_{e^\pm} \\ &\times G_{e^\pm}(E_{e^\pm},E'_{e^\pm};\vec{r},\vec{r}\,') \\ &\times \sum_f \mathrm{BR}(\phi_n\to f)\frac{dN^{(n)}_{f,e^\pm}}{dE'_{e^\pm}}(E'_{e^\pm}),\end{aligned} \quad (3.7)$$

where Ω_{tot} is defined in Eq. (2.4) and where τ_0 once again denotes the lifetime of the lightest ensemble constituent. In practice, we model the energy densities $\rho_n(\vec{r})$ [and thus $\rho_{\mathrm{tot}}(\vec{r})$] to be spatially distributed according to the NFW halo profile [29], and we evaluate the expressions in Eq. (3.7) numerically, using the publicly available PPPC4DMID package [31] to determine the electron and positron spectra at injection as well as to determine the effects of propagating these injected particles through the interstellar medium. However, as a cross-check, we have also verified that the resulting differential fluxes agree with the analytic results obtained using the approximate analytic Green's function [30] corresponding to the same choice of propagation model.

It is important to note the manner in which the DDM model parameters α, γ, and τ_0 appear in the expression in Eq. (3.7). In particular, it is only the combination $\alpha+\gamma$ which appears in the summand, as this combination dictates how the injected flux of $e^\pm$ due to ϕ_n decays scales across the ensemble. In so doing, this combination determines the *shape* of the observed $e^\pm$ flux spectra. Of course, the exponent α also implicitly appears in the overall normalization prefactor, since it affects the value of Ω_0 when Ω_{tot} is set equal to Ω_{CDM}. However, any change in this normalization factor due to a change in α can be absorbed into a corresponding rescaling of τ_0. Thus only $\alpha+\gamma$ and τ_0 serve as independent degrees of freedom insofar as the electron/positron fluxes are concerned. We will therefore express our results in terms of the combination $\alpha+\gamma$ in what follows, and perform a best-fit analysis to AMS-02 data in order to fix τ_0 for any choice of $\alpha+\gamma$. The particulars of this analysis will be discussed in Sec. V.

In addition to the primary contributions to $\Phi_{e^\pm}$ from dark-matter decay, we must also take into account the background contribution to these fluxes from astrophysical processes. In principle, these fluxes are specified by the choice of propagation model and the injection spectrum of $e^\pm$ from astrophysical sources, including both a primary contribution from objects such as supernova remnants and a secondary component due to the spallation of cosmic rays on the interstellar medium. In practice, however, the injection spectrum is not well known, and thus specifying a propagation model is still not sufficient to determine the astrophysical background fluxes of electrons and positrons at the location of the Earth. For this reason, following, e.g., Refs. [18,19,34], we adopt a background-flux model which provides a reasonably good empirical fit to the observed fluxes at low $E_{e^\pm}$, namely, the so-called "Model 0" presented by the FERMI Collaboration in Ref. [35]. These background fluxes are well described by the parametrizations [34]

$$\begin{aligned}\Phi^{\mathrm{BG}}_{e^-} &\approx k(10^{-4}) \\ &\times\left[\frac{82.0(E_{e^-}/\mathrm{GeV})^{-0.28}}{1+0.224(E_{e^-}/\mathrm{GeV})^{2.93}}\right]\mathrm{GeV}^{-1}\,\mathrm{cm}^{-2}\,\mathrm{s}^{-1}\,\mathrm{sr}^{-1}, \\ \Phi^{\mathrm{BG}}_{e^+} &\approx (10^{-4})\times\left[\frac{38.4(E_{e^+}/\mathrm{GeV})^{-4.78}}{1+0.0002(E_{e^+}/\mathrm{GeV})^{5.63}}\right. \\ &\left.+24.0(E_{e^+}/\mathrm{GeV})^{-3.41}\right]\mathrm{GeV}^{-1}\,\mathrm{cm}^{-2}\,\mathrm{s}^{-1}\,\mathrm{sr}^{-1},\end{aligned} \quad (3.8)$$

where k is a normalization coefficient which parametrizes the uncertainty in the background e^- flux. In our analysis, we allow k to fluctuate within the range $0.7 \le k \le 1.0$. This single degree of freedom clearly does not parametrize all of the uncertainties in the background fluxes. However,

it does provide some measure of flexibility for these fluxes which will be sufficient for our purposes. Indeed, although "Model 0" (which we use for calculating the astrophysical backgrounds) is quite different from the MED model (which we use to calculate those fluxes which originate from our DDM ensemble), "model 0" has the benefit that it successfully fits the measured background $e^{\pm}$ flux spectra in a suitable low-energy "control" region where data actually exists. A more complete discussion of the effects of uncertainties in the astrophysical background flux can be found in Ref. [36]. We will also discuss the treatment of these fluxes further in Sec. VI.

Finally, we remark that these interstellar background fluxes can be significantly modified by solar-modulation effects at very low energies $E_{e^{\pm}} \lesssim 10$ GeV. Indeed, for $E_{e^{\pm}} \lesssim 10$ GeV, the observed flux spectra at the top of the atmosphere can differ considerably from the functional forms given in Eq. (3.8). However, our main interest in this paper concerns the significantly higher energy range $20\ \text{GeV} \lesssim E_{e^{\pm}} \lesssim 1\ \text{TeV}$. Therefore, we shall disregard the effects of solar modulation in most of what follows. However, in all figures displayed in this paper, the results shown actually include this modulation effect, which we have calculated using the so-called force-field approximation [37]. Under this approximation, the observed fluxes are related to the interstellar fluxes via the modification [38]

$$\Phi_{e^{\pm}}^{\mathrm{BG,obs}} = \left(\frac{E_{e^{\pm}}}{E_{e^{\pm}} + e\phi_F}\right)^2 \Phi_{e^{\pm}}^{\mathrm{BG}}(E_{e^{\pm}} + e\phi_F), \tag{3.9}$$

where e is the electron charge and where $\phi_F = 550$ MeV is the value we adopt for the solar-modulation potential. A more complete discussion of solar-propagation modeling can be found in Ref. [39].

In summary, the total differential fluxes of cosmic-ray electrons and positrons in our DDM model is given by the sum of the corresponding signal contribution in Eq. (3.7) and the background contribution in Eq. (3.9):

$$\Phi_{e^{\pm}} = \Phi_{e^{\pm}}^{\mathrm{DDM}} + \Phi_{e^{\pm}}^{\mathrm{BG,obs}}. \tag{3.10}$$

Given these fluxes, the combined flux $\Phi_{e^+} + \Phi_{e^-}$ and the positron fraction $\Phi_{e^+}/(\Phi_{e^+} + \Phi_{e^-})$ directly follow.

IV. PHENOMENOLOGICAL CONSTRAINTS

In this section, we discuss the phenomenological constraints that we shall impose on our DDM model. In particular, we shall require that our general DDM model be consistent with

(i) limits from the PAMELA experiment [8] on the flux of cosmic-ray antiprotons;
(ii) limits from the FERMI-LAT experiment [10] on the observed gamma-ray flux, and especially on its diffuse isotropic component;
(iii) constraints [40] on the synchrotron radiation produced via the interaction between high-energy electrons and positrons within the galactic halo and background magnetic fields;
(iv) constraints on the ionization history of the universe, as recorded in the CMB, from existing anisotropy data and anticipated polarization data from Planck [14]; and
(v) constraints from the FERMI-LAT experiment [9] on the combined $e^{\pm}$ flux.

We shall now discuss each of these in turn.

A. Cosmic-ray antiproton constraints

As discussed in the Introduction, limits from PAMELA [8] on the flux of cosmic-ray antiprotons impose nontrivial constraints on dark-matter models which purport to explain the positron excess. These constraints are particularly stringent for dark-matter candidates which decay primarily either directly into quarks or gluons, or else into $W^{\pm}$ or Z bosons which in turn produce such particles with significant branching fractions via their subsequent decays.

However, these constraints are far less stringent for dark-matter candidates which decay primarily into charged leptons. For this reason, in our analysis we shall focus primarily on the case in which the constituents of the DDM ensemble decay leptonically, via processes of the form $\phi_n \to \ell^+\ell^-$, where $\ell = \{e, \mu, \tau\}$. In each case, we have used the PPPC4DMID package [31] to calculate the contribution to the cosmic-ray antiproton flux from the leptonic decays of our DDM ensemble, and we have verified that the antiproton flux lies well below experimental limits for all relevant antiproton energies. Indeed, this conclusion holds within all portions of the DDM parameter space which ultimately prove relevant for explaining the positron excess.

We emphasize that while other similar limits on decaying dark-matter particles exist—for example, constraints on the contributions of such particles to cosmic-ray antideuteron fluxes—these constraints do not significantly impact the parameter space of DDM ensembles whose constituents decay primarily via leptonic channels.

B. Gamma-ray flux constraints

The flux of gamma rays produced from annihilating or decaying dark-matter particles within the galactic halo is also tightly constrained by observation, as is the contribution from a cosmological population of decaying dark-matter particles to the isotropic gamma-ray flux. The latter constraints are typically more stringent for decaying dark-matter models [41,42]; moreover, they do not depend on the halo profile or other unknown properties of the dark-matter distribution within our galaxy. We therefore focus here on the isotropic gamma-ray constraints.

In general, the total contribution to the apparent isotropic gamma-ray flux from dark-matter decay receives two subcontributions:

$$\Phi_\gamma^{\rm Iso} = \Phi_\gamma^{\rm EGB} + 4\pi \frac{d\Phi_\gamma^{\rm DGB}}{d\Omega}\bigg|_{\rm min}. \qquad (4.1)$$

The first of these is the contribution from a cosmological population of decaying dark-matter particles to the true diffuse extragalactic gamma-ray flux. The second is the isotropic component of the residual contribution from decaying dark-matter particles in the galactic halo. This latter contribution includes individual contributions from prompt gamma-ray production and from gamma-ray production via the inverse-Compton scattering of $e^\pm$ produced by ϕ_n decays off background photons. We evaluate both of these contributions to the residual galactic background flux, as well as the truly diffuse extragalactic flux contribution, using the PPPC4DMID package [31]. Following the analysis in Ref. [42], we assume that the direction at which this latter contribution reaches a minimum is that opposite the galactic center.

Since there is substantial uncertainty in the background contribution to the isotropic gamma-ray flux from astrophysical sources (see, e.g., the various possible contributions discussed in Ref. [43]), we require as a consistency condition only that the contribution to this flux predicted from the decay of a given DDM ensemble alone not exceed the flux reported by the FERMI Collaboration [10]. In this manner, given a particular choice of model parameters, we determine a lower bound on the lifetime τ_0 of the lightest ensemble constituent. We do this by computing the goodness-of-fit statistic

$$\chi^2 = \sum_{i=1}^{N} \frac{(\Phi_i^{\rm obs} - \Phi_i^{\rm DDM})^2}{(\Delta\Phi_i^{\rm obs})^2}\,\Theta(\Phi_i^{\rm DDM} - \Phi_i^{\rm obs}), \qquad (4.2)$$

where the index i labels the energy bins into which the FERMI data are partitioned, where $\Phi_i^{\rm DDM}$ is the differential gamma-ray flux for bin i predicted by the DDM model in question, where $\Phi_i^{\rm obs}$ is the central value reported by FERMI for the gamma-ray flux in the corresponding bin, where $\Delta\Phi_i^{\rm obs}$ is the uncertainty in that central value, and where $\Theta(x)$ denotes the Heaviside theta function. We then compute a (one-sided) p value by comparing this goodness-of-fit statistic to a χ^2 distribution with N degrees of freedom, where $N = 9$ is the number of energy bins used in the FERMI gamma-ray analysis. Finally, we express this result in terms of the number of standard deviations away from the mean to which this p value would correspond for a (two-sided) Gaussian distribution. In this analysis, we adopt as our criterion for consistency with FERMI data the requirement that the isotropic gamma-ray flux contributed by the decays of the DDM ensemble constituents agree with the FERMI data to within 3σ. We note, however, that there also exist other methods [44] of using FERMI gamma-ray data to constrain the properties of decaying or annihilating dark matter.

C. Synchrotron radiation constraints

Gamma-ray signatures of this sort are not the only way in which photon signals constrain the properties of the dark matter. Indeed, synchrotron radiation produced via the interaction between high-energy electrons and positrons within the galactic halo and background magnetic fields can result in an observable radio signal. Observational limits on such a signal therefore constrain scenarios in which electrons and positrons are produced by a population of annihilating [45] or decaying [40,46] dark-matter particles. Constraints of this sort were derived in Ref. [40] for the case of a traditional dark-matter candidate χ which decays primarily into charged leptons, and, in particular, into e^+e^- pairs. For the choice of halo profile and propagation model we adopt here, it was shown that these constraints are generically subleading in comparison with direct constraints on the positron fraction for $m_\chi \gtrsim 11$ GeV. Indeed, the most stringent bound on the lifetime of any leptonically decaying χ with m_χ in this mass regime from synchrotron-emission considerations alone is $\tau_\chi \gtrsim 10^{26}$ s, again for a particle which decays essentially exclusively to e^+e^-. (The corresponding constraints on a particle with a significant branching fraction to $\mu^+\mu^-$ or $\tau^+\tau^+$ are even less stringent [46].) Since the above results hold for a single dark-matter component χ with $m_\chi \gtrsim 11$ GeV, they will necessarily hold component by component across our entire DDM ensemble so long as $m_0 \gtrsim 11$ GeV and $\alpha + \gamma < 0$. As we shall see, this latter condition is necessary in order to ensure that the injection energy decreases as a function of increasing mass within the ensemble. We therefore conclude that the synchrotron-emission constraints will always be less stringent than the limits on Φ_{e^+} from FERMI and AMS-02 data for any DDM ensemble satisfying these two constraints.

D. CMB ionization history constraints

In addition to direct limits on the observed gamma-ray and synchrotron fluxes, dark-matter decays in the early universe are also constrained by considerations related to the CMB. In particular, high-energy photons, electrons, and positrons produced as a result of dark-matter decays in the early universe can alter the ionization history of the universe, thereby leaving an observable imprint on the CMB. That no such imprint has been observed in CMB data implies stringent constraints [47–52] on dark-matter annihilation and decay. Forthcoming CMB-polarization data from Planck will improve upon these limits, and projections based on the expected performance of the Planck satellite for the case of a single long-lived dark-matter particle χ have been assessed by a number of authors [52].

Broadly speaking, the results of these studies indicate that such a dark-matter particle χ must have a lifetime $\tau \gtrsim 10^{26}$ s if it is to have a cosmological abundance $\Omega_\chi \sim \mathcal{O}(1)$, and that the upper limit on the present-day abundance of such a

long-lived particle drops rapidly as the lifetime of the particle decreases. These studies also indicate that the upper bound on Ω_χ is not particularly sensitive to the mass of χ.

A precise determination of the corresponding limits on the parameter space of any given DDM scenario would require a detailed reanalysis of the ionization history of the universe in the presence of a DDM ensemble. However, we can derive a rough criterion for consistency with CMB data from the usual CMB limits on decaying dark-matter particles based on the observation that such limits essentially constrain the energy injection from dark-matter decays [47], and that these constraints are not particularly sensitive to the mass of the decaying particle. Indeed, for any such particle with a lifetime $\tau_\chi \gtrsim 10^{13}$ s, the projected Planck limits derived in Ref. [52] essentially amount to a constraint $\Omega_\chi \Gamma_\chi \lesssim 3 \times 10^{-26}\ \mathrm{s}^{-1}$. We can therefore establish a rough criterion for consistency with CMB data by imposing an analogous condition on the total energy injection from the DDM ensemble as a whole:

$$\xi \equiv \sum_{n=0}^{n_{\max}} \Omega_n \Gamma_n \lesssim 3 \times 10^{-26}\ \mathrm{s}^{-1}. \tag{4.3}$$

Indeed, for the specific case of a DDM ensemble parametrized as in Sec. II, the quantity ξ takes the form

$$\xi = \frac{\Omega_0}{\tau_0} \sum_{n=0}^{N_{\mathrm{CMB}}} \left(1 + n^\delta \frac{\Delta m}{m_0}\right)^{\alpha+\gamma} \tag{4.4}$$

where

$$N_{\mathrm{CMB}} \equiv \left(\frac{m_0}{\Delta m}\right)^{1/\delta} \left[\left(\frac{\tau_0}{t_{\mathrm{CMB}}}\right)^\gamma - 1\right]^{1/\delta} \tag{4.5}$$

is the highest value of the index n for which ϕ_n has a lifetime longer than a fiducial early time $t_{\mathrm{CMB}} \sim 10^{11}$ s. This is approximately the time before which decays have little effect on the CMB. Note that since $\alpha + \gamma < 0$, the individual constituent contributions to ξ necessarily decrease as a function of increasing mass within the ensemble. This helps soften the sensitivity of ξ to the precise value of N_{CMB}.

In Fig. 1, we show contours of the energy-injection parameter ξ in the $(\tau_0,\ \alpha + \gamma)$ plane for $\alpha = -3$ (left panel) and $\alpha = -2$ (right panel). For both panels, we have set $\Delta m = 1$ GeV, $\delta = 1$, and $m_0 = 500$ GeV, although we emphasize that the results shown here are essentially insensitive to the choice of m_0 within the range $100\ \mathrm{GeV} \lesssim m_0 \lesssim 1500\ \mathrm{GeV}$. The hatched region demarcated by the solid black curve is the region of parameter space excluded by the CMB-consistency criterion in Eq. (4.3). It is clear from the figure that our CMB criterion imposes a nontrivial constraint on the parameter space of our DDM model. Indeed, for the range of values of τ_0 relevant for reproducing the observed positron excess, consistency with this criterion essentially requires $\alpha + \gamma \lesssim -1$ and a lifetime $\tau_0 \gtrsim 10^{25}$ s.

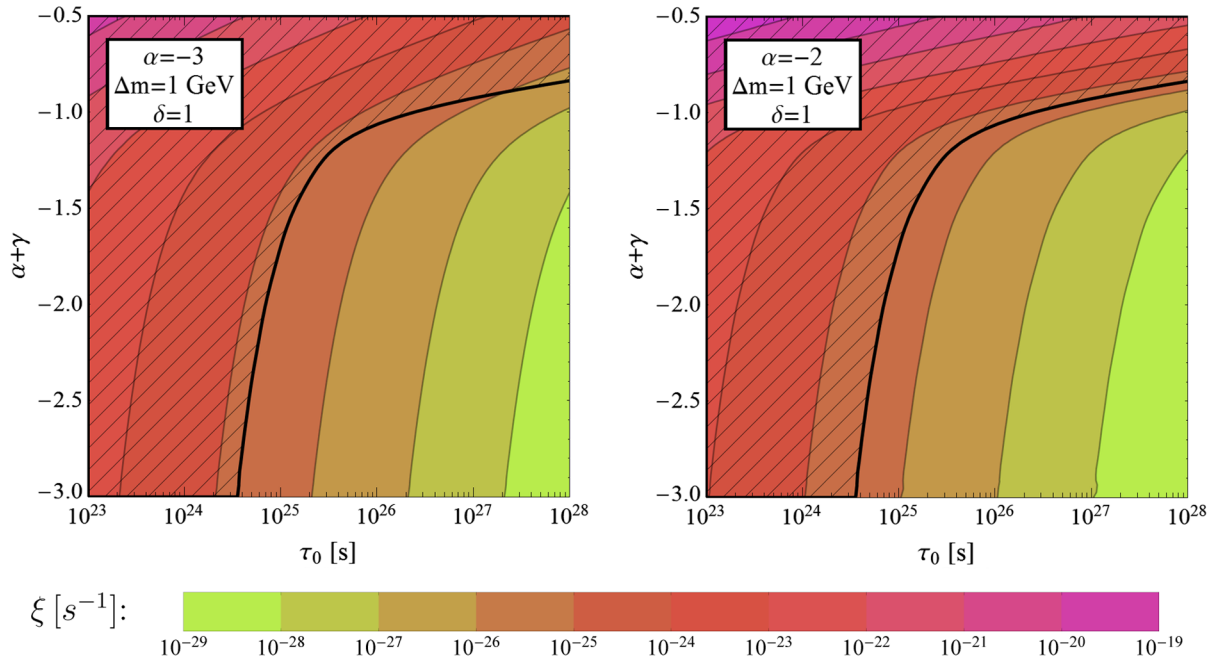

FIG. 1 (color online). The region of $(\tau_0,\ \alpha + \gamma)$ DDM parameter space excluded by prospective CMB constraints on modifications of the ionization history of the universe due to the presence of a decaying DDM ensemble parametrized as in Eqs. (2.1) and (2.2). The results shown in the left and right panels correspond, respectively, to $\alpha = -3$ and $\alpha = -2$. The contours shown indicate the value of the injection-energy parameter ξ, and the hatched region demarcated by the solid black curve is the region of parameter space excluded by the CMB-consistency criterion in Eq. (4.3).

E. Combined electron/positron-flux constraints

Finally, we require that the combined $e^{\pm}$ flux from the DDM ensemble agree with the combined $e^{\pm}$ flux reported by the FERMI Collaboration [9] to within 3σ. Note that we evaluate the goodness of fit for this combined flux in the same manner as for the gamma-ray flux, except that the corresponding χ^2 statistic does not include the Heaviside-theta-function factor which appears in Eq. (4.2).

V. RESULTS

Having outlined the phenomenological constraints that we require our DDM model to satisfy, we now turn to the main issue of this paper: to what extent can we construct DDM models of the sort outlined in Sec. II which not only satisfy these constraints but also agree with the recent data from the AMS-02 experiment concerning the positron fraction for energies up to $E_{e^+} \approx 350$ GeV? And even more importantly, to what extent can we then *predict* the behavior of the positron fraction for even higher energies, in the range $350\ \text{GeV} \lesssim E_{e^+} \lesssim 1\ \text{TeV}$?

In order to address these questions, we adopt the following procedure. First, as discussed in Sec. II, we survey over the parameter space (α, γ, m_0) of our DDM model, fixing $\Delta m = 1$ GeV and $\delta = 1$. For each point (α, γ, m_0) in the DDM parameter space, we then perform a best-fit analysis for the lifetime τ_0 of the lightest mode as well as for the overall normalization factor k associated with the background electron flux (restricted to the range $0.7 \leq k \leq 1.0$). Finally, we determine the minimum statistical significance with which the corresponding ensemble reproduces the results obtained by the AMS-02 experiment within the energy range $20\ \text{GeV} < E_{e^\pm} < 350\ \text{GeV}$ while simultaneously satisfying all of our consistency criteria. Once again, as with the combined $e^{\pm}$ flux, we evaluate the goodness of fit for the positron fraction in the same manner as for the gamma-ray flux, except that the corresponding χ^2 statistic does not include the Heaviside-theta-function factor which appears in Eq. (4.2).

Our results are as follows. For a DDM ensemble whose constituents ϕ_n are bosonic and decay either primarily to e^+e^- or primarily to $\tau^+\tau^-$, we find no combination of parameters for which our consistency criteria are satisfied and the ensemble simultaneously yields a positron-fraction curve which accords with AMS-02 results within 5σ. In particular, we find that the $\phi_n \to \tau^+\tau^-$ channel tends to overproduce gamma rays while the $\phi_n \to e^+e^-$ channel tends to produce too hard an energy spectrum—even within the context of a DDM ensemble.

By contrast, for an ensemble whose constituents decay primarily to $\mu^+\mu^-$, we find that there exist large regions of parameter space within which all of our criteria are satisfied and within which the DDM ensemble provides a good fit to AMS-02 data. In Fig. 2, we indicate these regions of

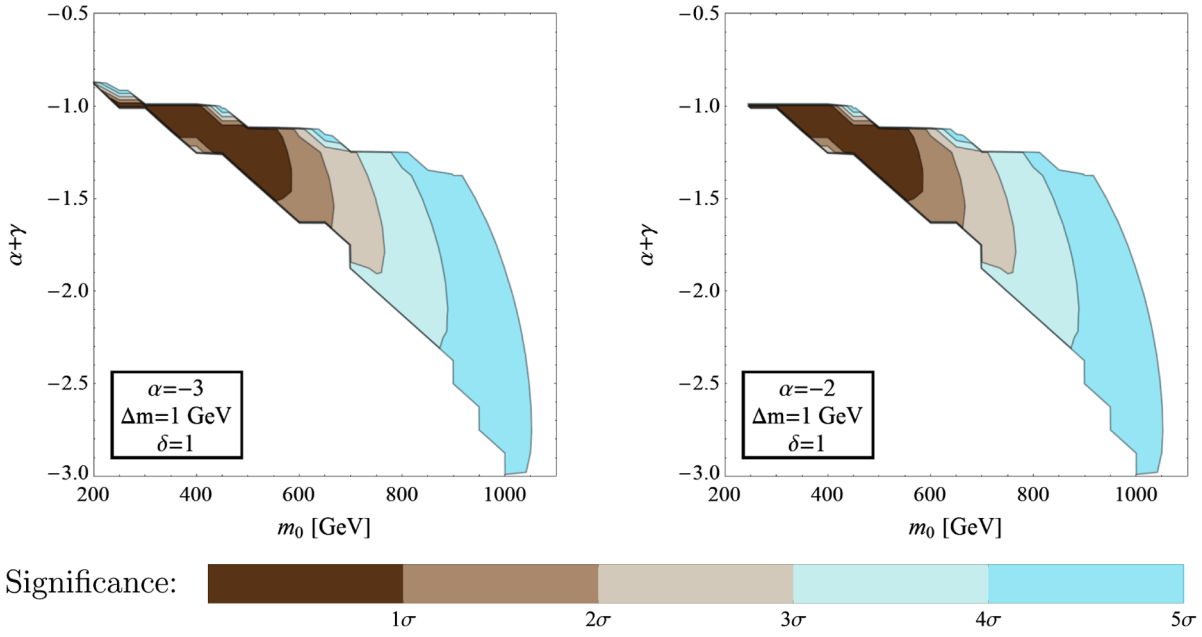

FIG. 2 (color online). Contours of the minimum significance level with which a given DDM ensemble is consistent with AMS-02 data, plotted within the $(m_0, \alpha + \gamma)$ DDM parameter space for $\alpha = -3$ (left panel) and $\alpha = -2$ (right panel). The colored regions correspond to DDM ensembles which successfully reproduce the AMS-02 data while simultaneously satisfying all of the applicable phenomenological constraints outlined in Sec. IV, while the white regions of parameter space correspond to DDM ensembles which either cannot simultaneously satisfy these constraints or which fail to match the AMS-02 positron-excess data at the 5σ significance level or greater. The slight difference between the results shown in the two panels is a consequence of the differences in the CMB constraints for the two corresponding values of α.

$(m_0, \alpha + \gamma)$ space by shading them according to the significance level within which the decaying DDM ensemble is capable of reproducing the positron-fraction results from AMS-02. The results in the left and right panels correspond to the choices $\alpha = -3$ and $\alpha = -2$, respectively. The white regions, by contrast, indicate those regions of parameter space within which our consistency criteria cannot simultaneously be satisfied while at the same time yielding a positron fraction which agrees with AMS-02 at the 5σ significance level or better. Note that the difference between the results shown in the two panels is extremely slight, and is due to a slight weakening of the CMB constraint with decreasing α.

We see, then, that a DDM ensemble whose constituent particles decay primarily to $\mu^+\mu^-$ can indeed account for the observed positron excess while at the same time satisfying other phenomenological constraints on decaying dark matter. The underlying reason for this success is easy to understand upon comparison with the case of a traditional dark-matter candidate with the same decay phenomenology. In a nutshell, the $e^\pm$ injection spectra associated with traditional dark-matter candidates with the same decay phenomenologies are generally too hard, and thus cannot match the softer AMS-02 data after propagation through the ISM. By contrast, in the DDM framework, the total dark-matter cosmological abundance $\Omega_{\rm CDM}$ is partitioned across an ensemble of individual constituents with different masses. This in turn leads to a softening of the resulting $e^\pm$ injection spectra. Furthermore, a traditional dark-matter candidate must generally be quite heavy in order to reproduce the observed positron fraction, with a mass $m_\chi \gtrsim 1$ TeV. For such a heavy dark-matter candidate, it is difficult at the same time to reproduce the combined FERMI flux $\Phi_{e^+} + \Phi_{e^-}$; moreover, for such candidates, constraints related to the gamma-ray flux are quite severe. However, we see from Fig. 2 that the preferred region of parameter space for our DDM model is one in which a significant fraction of the dark-matter cosmological abundance $\Omega_{\rm CDM}$ is carried by constituents with masses in the range 200 GeV $\lesssim m_n \lesssim$ 800 GeV. For such light particles, the gamma-ray constraints are less severe.

It is this observation which lies at the heart of the phenomenological success of the DDM ensemble. Moreover, according to the results of Ref. [26], the preferred regions of DDM parameter space indicated in Fig. 2 correspond directly to those regions in which the full DDM ensemble contributes meaningfully to the cosmological dark-matter abundance $\Omega_{\rm CDM}$ (as opposed to regions in which the single most-abundant constituent effectively carries the entirety of $\Omega_{\rm CDM}$). Thus, we see that it is the full set of degrees of freedom within the DDM ensemble which plays a role in achieving this outcome.

Having demonstrated that DDM ensembles can successfully reproduce the positron fraction reported by AMS-02, we now turn to the all-important question of how the predicted DDM positron fraction behaves at energies $E_e > 350$ GeV. In this way, we will not only be probing the phenomenological predictions of the DDM framework, but we also will be determining the extent to which further data from AMS-02 or from other forthcoming cosmic-ray experiments might serve to distinguish between DDM ensembles and other explanations of the positron excess.

Our results are shown in Fig. 3. In this figure, superimposed on the actual experimental data, we have plotted the predicted combined flux and positron fraction which correspond to a variety of DDM parameter choices that lie

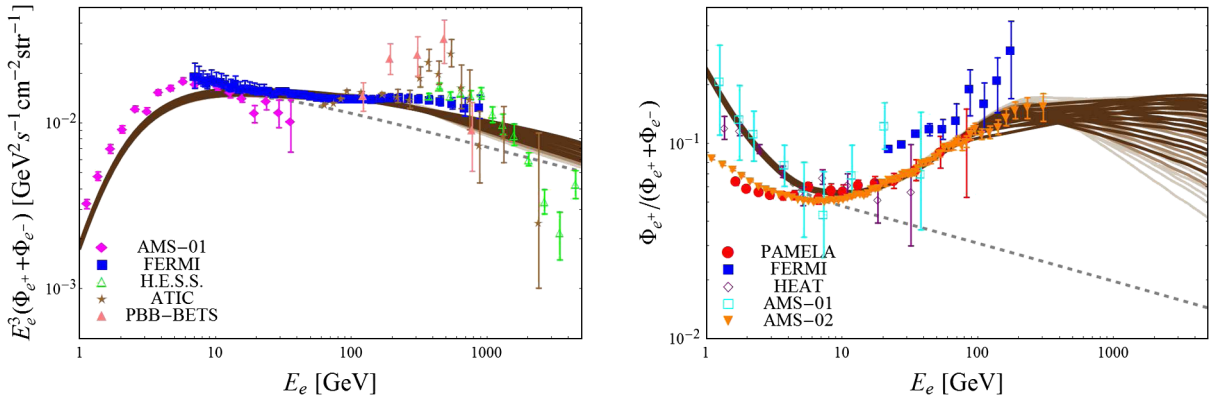

FIG. 3 (color online). Predicted combined fluxes $\Phi_{e^+} + \Phi_{e^-}$ (left panel) and positron fractions $\Phi_{e+}/(\Phi_{e^+} + \Phi_{e^-})$ (right panel) corresponding to the DDM parameter choices lying within those regions of Fig. 2 for which our curves agree with AMS-02 data to within 3σ. These curves are therefore all consistent with current combined-flux data to within 3σ and also consistent with current positron-fraction data to within 3σ (with the color of the curve indicating the precise quality of fit, using the same color scheme in Fig. 2). These curves are also consistent with all other applicable phenomenological constraints discussed in Sec. IV. However, despite these constraints, the behavior of the positron-fraction curves beyond $E_{e^\pm} \sim 350$ GeV is entirely unconstrained except by the internal theoretical structure of the DDM ensemble. Their relatively flat shape in this energy range thus serves as a prediction (and indeed a "smoking gun") of the DDM framework. Data from AMS-02 [1], HEAT [2], AMS-01 [3], PAMELA [6], FERMI [7,9], PBB-BETS [53], ATIC [54], and HESS [55] are also shown for reference.

within those regions of Fig. 2 for which our curves agree with AMS-02 data to within 3σ. The color of each such curve reflects the significance level to which the predicted and observed positron fractions agree, using the same color scheme as in Fig. 2. We emphasize once again that the values of τ_0 and k for each curve shown in Fig. 3 are those for which the best fit to the positron fraction is obtained, irrespective of the goodness of fit to the combined $e^{\pm}$ flux, provided that this goodness of fit corresponds to a statistical significance of at most 3σ. As a result, the curves shown in the left panel of this figure essentially all deviate from FERMI data at the 3σ significance level. However, substantially improved consistency with FERMI data can easily be achieved without significantly sacrificing consistency with AMS-02 data—e.g., by employing an alternative fitting procedure involving a combined fit to both data sets simultaneously. Note also that the fit to FERMI data depends on a number of assumptions concerning the astrophysical background flux, and not merely its normalization; hence small deviations from FERMI $\Phi_{e^+} + \Phi_{e^-}$ results are not necessarily to be taken as a sign of tension with data.

We immediately see from Fig. 3 that DDM ensembles give rise to unusual and distinctive positron-fraction curves whose behaviors at high energies differ significantly from those obtained for traditional dark-matter models. Indeed, traditional dark-matter models for explaining the observed positron excess predict a rather pronounced downturn at $E_{e^\pm} \lesssim m_\chi$ (for annihilating dark matter) or $E_{e^\pm} \lesssim m_\chi/2$ (for decaying dark matter), where m_χ denotes the mass of the dark-matter particle. By contrast, as we see in Fig. 3, DDM ensembles give rise to positron-fraction curves which either decline only gradually or remain effectively flat for $E_{e^\pm} \gtrsim 350$ GeV. Indeed, we see that $\Phi_{e^+}/(\Phi_{e^+} + \Phi_{e^-}) \lesssim 0.2$ over this entire range. In principle, of course, DDM ensembles can give rise to positron-fraction curves exhibiting a broad variety of shapes and features. However, imposing the requirements that the positron fraction and combined $e^{\pm}$ flux agree with current data substantially limits the high-energy behaviors for the resulting positron fraction, permitting only those curves for which this fraction levels off and remains relatively constant as a function of energy.

Since no sharp downturn in the positron fraction appears consistent within the DDM framework, we may take this to be an actual prediction of the framework. The presence or absence of such a downturn therefore offers a powerful tool for distinguishing decaying DDM ensembles from other dark-matter explanations of the positron excess. Even more importantly, however, we observe that a positron fraction which falls only gradually or which remains effectively constant for $E_{e^\pm} \gtrsim 350$ GeV can be achieved only in a scenario in which an ensemble of dark-matter states with different masses and decay widths act together in coordinated fashion in order to support the positron-fraction function against collapse and to carry it smoothly into this higher energy range. This behavior, if eventually observed experimentally, can therefore be taken as a virtual "smoking gun" of Dynamical Dark Matter.

This claim, of course, rests upon the fundamental assumption that we are attributing the positron excess to dark-matter physics. As we have indicated above, it is always possible that some configuration of pulsars or other astrophysical sources can also provide part or all of the explanation for the observed positron excess. Given this observation, it may initially seem that our conclusions regarding the spectra predicted by the DDM framework may be somewhat moot. However, the success of the DDM framework not only in accommodating the existing positron data but also in predicting the continuation of the positron excess out to 1 TeV can be taken, conversely, as indicating that one need not be forced into a conclusion involving traditional astrophysical sources should such phenomena be observed experimentally. Indeed, as we have shown, there exists a well-motivated dark-matter framework—namely that involving a DDM ensemble obeying well-ordered scaling relations—which can easily do the job.

VI. VARYING THE INPUT ASSUMPTIONS

In the previous section, we showed that the DDM framework can naturally accommodate the positron excess, that this framework actually predicts that the positron excess will continue out to energies of at least approximately $E \sim 1$ TeV, and that any future experimental verification of this prediction can actually be taken (within the confines of dark-matter interpretations of the positron excess) as a "smoking gun" for DDM. However, there are a number of input assumptions which have either explicitly or implicitly played a role in our analysis—some of these concern the structure of the DDM ensemble itself, while others concern the background astrophysical environment whose properties also enter into our calculations. It is therefore critical that we understand the extent to which our results are robust against variations in these input assumptions.

A. Varying the structure of the DDM ensemble

As discussed in Sec. II, our DDM ensemble can be parametrized in terms of five fundamental parameters $\{\alpha, \gamma, \delta, m_0, \Delta m\}$. (The remaining parameters $\{\Gamma_0, \Omega_0\}$ are then essentially determined through the "normalization" conditions discussed earlier.) In the analysis we have presented thus far, we have allowed α, γ, and m_0 to vary, but we have taken $\delta = 1$ and $\Delta m = 1$ GeV as fixed benchmarks. Since there is nothing in the DDM framework which requires these particular values, it is reasonable to ask what new effects might emerge if these values are altered.

The parameters Δm and δ play independent but correlated roles: both appear in Eq. (2.1) and together they parametrize the density of states in the DDM ensemble.

Increasing δ or Δm has the effect of increasing the masses of the heavier DDM constituents relative to the lighter ones, thereby potentially diminishing their effects on low-energy physics. Indeed, for sufficiently large Δm, our DDM ensemble essentially acts as a traditional single-particle dark sector as far as most low-energy effects are concerned. By contrast, decreasing δ or Δm has the reverse effect. Indeed, in the $\Delta m \to 0$ limit, the states in the DDM ensemble form a continuum, and in practice such "continuum" behavior can be expected whenever Δm is smaller than the scale set by the energy resolution of the relevant cosmic-ray detectors.

In our analysis thus far, we were motivated to take $\delta = 1$ because this is the value which arises in certain well-motivated realizations of DDM ensembles involving large extra spacetime dimensions [22,23]. However, our choice of $\Delta m = 1$ GeV was made on purely aesthetic grounds, as a small value of this size ensures that a large portion of the DDM ensemble plays a role in contributing to the relevant cosmic-ray fluxes. It is therefore interesting to understand the extent to which our predictions remain valid even if Δm exceeds this value.

In Fig. 4, we show the fluxes which emerge from a variety of DDM ensembles corresponding to different values of Δm, while the remaining DDM parameters are held fixed at values which ensure a successful fit to AMS-02 data for $\Delta m = 1$ GeV. As we see from this figure, increasing the value of Δm causes the resulting fluxes to increasingly deviate from the existing AMS-02 data, particularly at the highest energies for which such data is available. This is particularly dramatic for the positron-fraction data; indeed, increasing the value of Δm ultimately reintroduces the characteristic downturn that is normally associated with traditional single-component dark-matter candidates. As we see, it is only by taking Δm sufficiently small that the predicted positron fraction can match all of the AMS-02 data. This is precisely the "DDM limit" in which a large portion of the DDM ensemble plays an active role in contributing to the cosmic-ray fluxes at these energies.

This observation demonstrates that there is a strong correlation between obtaining a successful fit to the AMS-02 data and having a dark sector such as a DDM ensemble in which a relatively large number of dark-matter states actually contributes to the cosmic-ray fluxes at these energies. But what is particularly remarkable about the results shown in Fig. 4 is the existence of a second, independent correlation: a successful fit to the entirety of available AMS-02 data is also correlated with the absence of a sharp downturn in the positron fraction out to energies $E_{e^\pm} \sim 1$ TeV. Indeed, setting Δm to any value less than the maximum value that will fit the existing AMS-02 data causes the corresponding positron fraction to exhibit at most a gently declining plateau out to $E_{e^\pm} \sim 1$ TeV. In an arbitrary hypothetical multicomponent theory of dark matter, this second correlation need not have existed, but its emergence in the DDM framework is ultimately a consequence of the tight internal scaling structure of the DDM ensemble. It is this "rigidity" of the DDM ensemble—i.e., its inability to fit the existing AMS-02 data while simultaneously producing an immediate downturn in the positron fraction at higher energies—which is the underlying reason that the DDM framework yields such "smoking gun" predictions about the positron fraction at higher energies. (In this context we remark that although

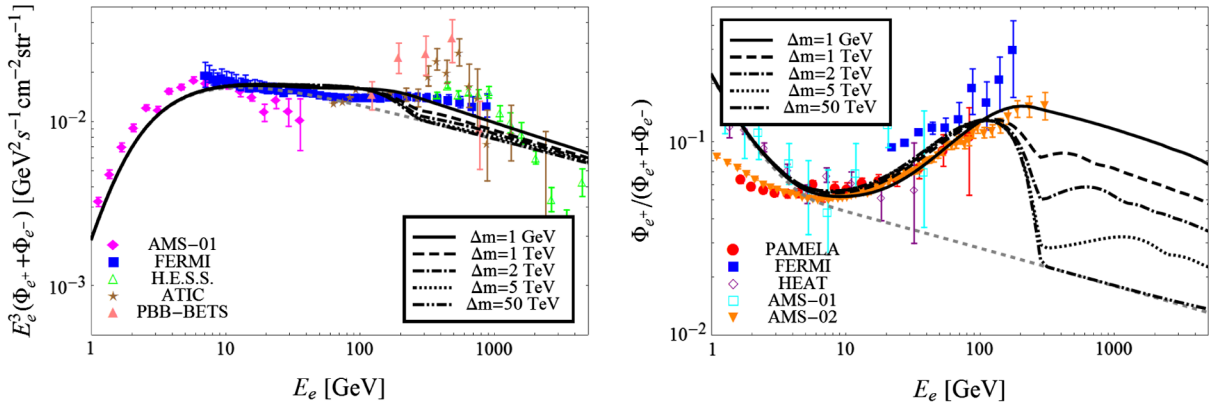

FIG. 4 (color online). The combined flux $\Phi_{e^+} + \Phi_{e^-}$ (left panel) and positron fraction $\Phi_{e+}/(\Phi_{e^+} + \Phi_{e^-})$ (right panel) corresponding to DDM parameter choices $\Delta m = \{10^{-3}, 1, 2, 5, 50\}$ TeV. For these plots we have held the other DDM parameters fixed at reference values $\alpha = -2$, $\gamma = 0.5$, $\delta = 1$, $m_0 = 600$ GeV, and $\tau_0 = 3.23 \times 10^{26}$ s, and we have taken $k = 0.9$ in Eq. (3.8). As expected, passing to larger values of Δm has the effect of decreasing the flux contributions from heavier states in the DDM ensemble; the resulting fluxes thus increasingly fail to match the existing highest-energy AMS-02 data for the positron fraction and at the same time begin to exhibit the characteristic downturn in the positron fraction that is normally associated with traditional single-component dark-matter candidates. Indeed, only by taking Δm sufficiently small does the predicted positron fraction match all of the AMS-02 data. However, a large portion of the DDM ensemble then plays an active role in contributing to these fluxes, whereupon the internal structure of the ensemble itself compels the positron fraction to remain significantly above background—even out to energies $E_{e^\pm} \sim 1$ TeV—without any sharp downturn.

we have taken $m_0 = 600$ GeV for the curves in Fig. 4, altering m_0 does not change this conclusion and would in fact cause difficulties satisfying our other constraints on the total gamma-ray flux or the total $\Phi_{e^+} + \Phi_{e^-}$ flux.) Thus, this correlation is relatively robust against variations in Δm, and we expect it to hold for all values Δm which are sufficiently small as to permit a successful fit to the AMS-02 data.

In this connection, it is perhaps also worth commenting on the role played by the quantity $n_{\rm max}$ which truncates our sums over DDM constituents in Eqs. (2.4) and (3.5), and so forth. At first glance, it might seem that $n_{\rm max}$ is yet another free parameter in the DDM framework. Even worse, if we attempt to interpret $n_{\rm max}$ literally as the number of DDM states which contribute to the cosmic-ray fluxes, we might be tempted to view any fit requiring a very large value of $n_{\rm max}$ as somehow uninteresting, since it might be expected on general grounds that fits to data can always be performed with arbitrary precision if we have sufficiently many degrees of freedom at our disposal. While these worries would certainly be valid for an arbitrary hypothetical multicomponent theory of dark matter, the important point here is that our dark sector is not just a random collection of individual states with arbitrary, freely adjustable masses and decay widths. Instead, these states are part of a DDM *ensemble* which is collectively constrained by scaling relations of the sorts described in Sec. II. Indeed, in the DDM framework, the dark sector is parametrized in terms of relatively few degrees of freedom (such as α, γ, and m_0, as discussed above), and these quantities are chosen in such a way as to eliminate any theoretical or numerical sensitivity to the cutoff $n_{\rm max}$. At a practical level, this means that the cosmic-ray flux contributions from all DDM states are completely and simultaneously fixed once these few parameters are specified, and that successively heavier DDM states make increasingly smaller contributions to these fluxes in such a way that all sums are convergent as $n_{\rm max} \to \infty$.

B. Varying the astrophysical modeling

Thus far we have concentrated on input assumptions associated with our DDM ensembles. However, there were also a number of implicit assumptions of a purely astrophysical nature. In particular, in this category, two assumptions stand out:

(i) We used a particular astrophysical propagation model (the so-called "MED" propagation model) in order to calculate our DDM-produced cosmic-ray fluxes.

(ii) We assumed a particular dark-matter halo profile (the so-called "NFW" profile) for our DDM ensemble.

As discussed in Secs. II and III, both of these assumptions were implicitly part of the flux calculations leading to the results in Fig. 2. However, neither of these assumptions is required on theoretical grounds, and in each case there exist alternative models which might have been chosen. For example, rather than adopt the MED propagation model, we could have adopted its siblings, the MIN or MAX propagation models [32,33]. Together, the MIN, MED, and MAX models reside within an entire class of propagation models which differ in (and are therefore effectively parametrized in terms of) the degree to which the input fluxes are "processed" (or effectively shifted downwards in energy) in passing through the interstellar medium, with the MIN (MAX) propagation model tending to minimize (maximize) the resulting fluxes of charged cosmic-ray particles subject to certain phenomenological constraints. Likewise, rather than adopt the NFW dark-matter halo, we could just as easily have adopted any of a number of other halo profiles. For example, one well-motivated choice might be the so-called "isothermal" dark-matter halo [56]—this is nothing but the density distribution exhibited by an isothermal, self-gravitating system of particles, and leads to a velocity dispersion which is essentially constant at large radii. Note that the isothermal dark-matter halo is generally smoother (i.e., less "cuspy") than the NFW halo at small radii and thus forms a nice counterpoint to the NFW halo profile.

In Fig. 5, we show the degree to which the results in Fig. 2 would be altered by such replacements. As we see from Fig. 5, the effect of replacing the MED propagation model with the MIN propagation model is quite dramatic and results in a near-total elimination of the allowed DDM parameter space, while replacement with the MAX propagation model does not dramatically alter the allowed region of DDM parameter space and merely changes the calculated quality of fit to AMS-02 data within this region. These results are relatively easy to understand. Broadly speaking, the effect of propagation on the injected fluxes through the interstellar medium is to increase the contribution to $\Phi_{e^\pm}(E_{e^\pm})$ at low $E_{e^\pm}$ from injected $e^\pm$ with an injection energy $E'_{e^\pm} > E_{e^\pm}$. Moreover, this effect becomes increasingly pronounced at higher $E'_{e^\pm}$. The collective contribution to $\Phi_{e^\pm}$ from the heavier constituents in the DDM ensemble is therefore greater at low $E_{e^\pm}$ for propagation models such the MAX model, in which the processing of the $e^\pm$ injection spectra by the interstellar medium is more pronounced. As we have seen, this contribution is ultimately responsible for the all-important softening of the $\Phi_{e^\pm}$ flux spectra which renders these spectra compatible with the AMS-02 data. Therefore, the increased processing of the injection spectrum by the interstellar medium in the MAX model relative to the MED model can compensate to some degree for the hardening of the injection spectrum which results from an increase in m_0, as shown in Fig. 4. By contrast, use of the MIN propagation model has the effect of minimizing the contributions to the low-energy $e^\pm$ fluxes from the heavier DDM ensemble components. The resulting near-total elimination of the allowed DDM parameter space therefore can be taken as yet another feature highlighting the critical role of the entire DDM ensemble (and not just its lightest component) in producing a successful fit to AMS-02 data.

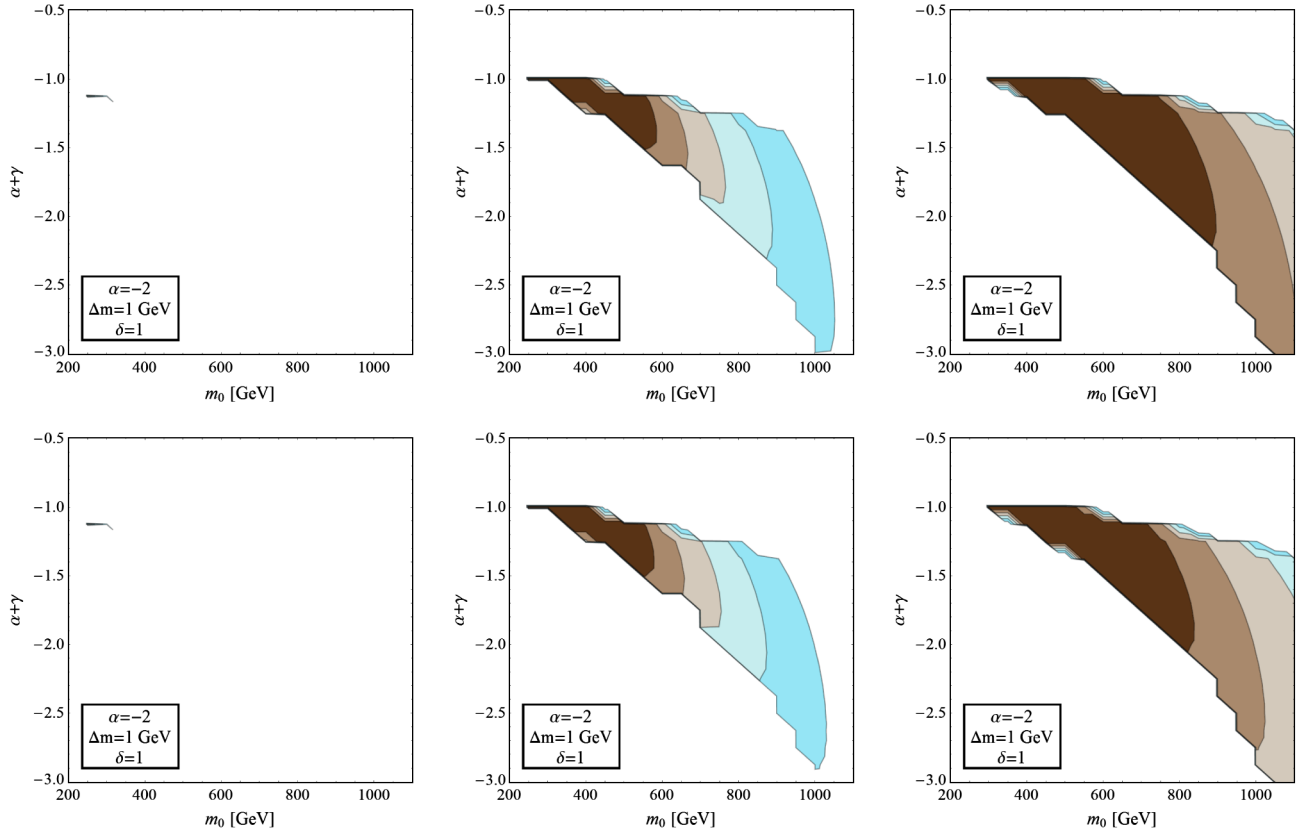

FIG. 5 (color online). Contours of the minimum significance level with which a given DDM ensemble is consistent with AMS-02 data, plotted exactly as in Fig. 2 but with $\alpha = -2$ only. The plots in the (left, middle, right) column are, respectively, calculated using the (MIN, MED, MAX) propagation model, while those in the (top, bottom) row are, respectively, calculated assuming an (NFW, isothermal) dark-matter halo. Thus the upper middle panel is identical to the right panel of Fig. 2, and is reproduced here for comparison purposes. We see that while the MIN propagation model results in a near-total elimination of the allowed DDM parameter space, the MED and MAX propagation models result in allowed parameter spaces which are roughly equivalent, differing only in their qualities of fit to the AMS-02 data. Likewise, we see that our results are almost completely insensitive to the particular form of the dark-matter halo assumed.

The other lesson that can be drawn from Fig. 5 is that our results are not particularly sensitive to the choice of halo profile. This indicates that our results are indeed properties of the DDM framework rather than properties of the specific halo profile chosen. The primary reason for this halo insensitivity is that the dominant contribution to Φ_{e^+} and Φ_{e^-} in the DDM framework is the result of dark-matter decay rather than dark-matter annihilation. The contribution to Φ_{e^+} or Φ_{e^-} from a decaying dark-matter particle ϕ is proportional to its density ρ_ϕ, whereas for an annihilating particle it is proportional to ρ_ϕ^2. These fluxes are consequently far less sensitive to the shape of the dark-matter halo in the former case than in the latter. Likewise, the dominant constraints on decaying dark-matter models of the positron excess come from considerations which depend either very weakly (or not at all) on the shape of the galactic dark-matter halo, such as the diffuse extragalactic gamma-ray flux and the properties of the CMB radiation.

In Fig. 6, we show the fluxes which result from the use of the MIN and MAX propagation models within the corresponding allowed parameter spaces shown in Fig. 5. As we saw in Fig. 5, use of the MIN propagation model results in only a small surviving sliver of DDM parameter space; this in turn leads to a fairly sharp set of flux predictions in Fig. 6. By contrast, use of the MAX propagation model leads to a set of possible fluxes in Fig. 6 which are even somewhat broader in their allowed behaviors than those which appear in Fig. 3 for the MED propagation model. Despite these differences, however, we once again see that the primary prediction of the DDM framework—that the positron fraction will continue to exhibit a surplus out to the higher energies $E_{e^+} \sim 1$ TeV without exhibiting a sharp downturn—continues to hold in all cases. Indeed, even the steepest allowed decline exhibited in the MAX case continues to be a relatively slow one in which the positron flux reaches its expected background value only at energies well beyond $E_{e^\pm} \sim 1$ TeV.

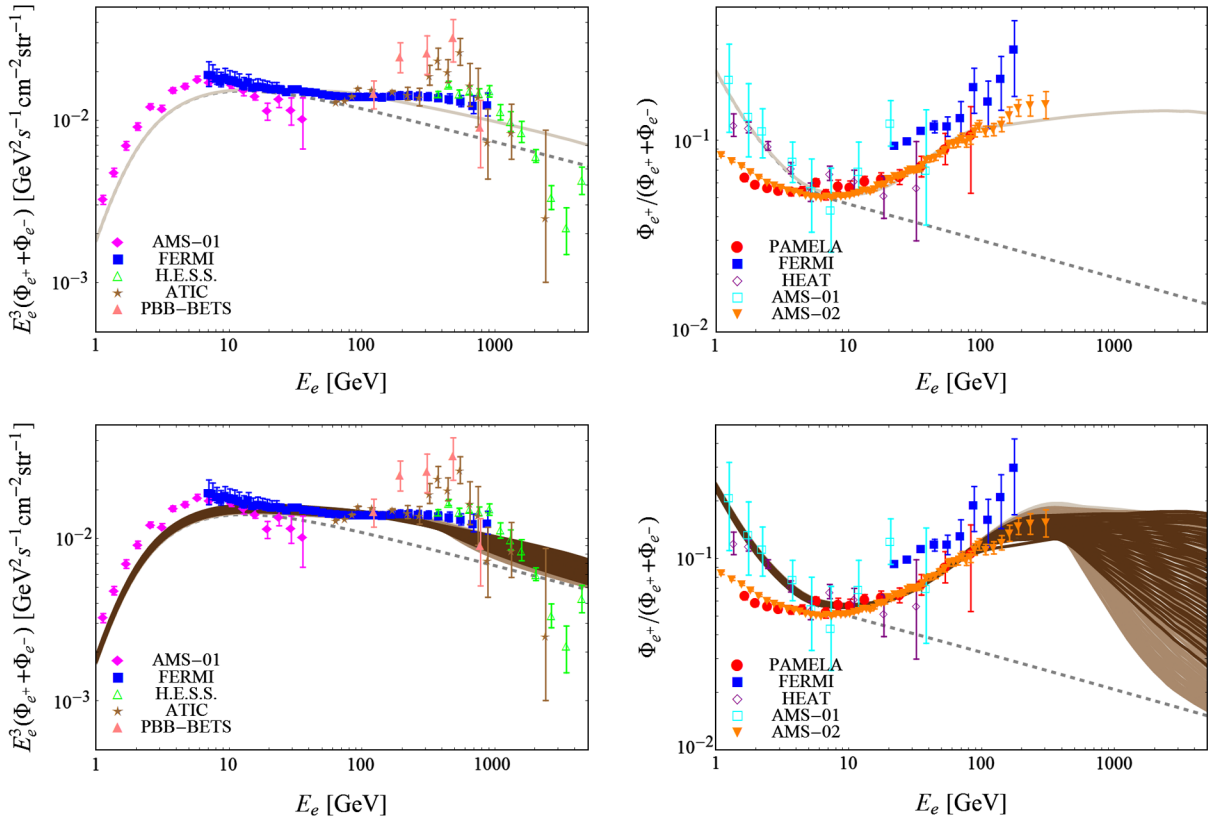

FIG. 6 (color online). The combined flux $\Phi_{e^+} + \Phi_{e^-}$ (left panels) and positron fraction $\Phi_{e+}/(\Phi_{e^+} + \Phi_{e^-})$ (right panels) corresponding to the DDM parameter choices illustrated in Fig. 5 for the MIN propagation model (top row) and the MAX propagation model (bottom row). Even though the MAX propagation model allows considerably greater flexibility in terms of the behavior of the positron fraction than the MIN or MED propagation models, even this case does not permit a sudden, sharp downturn in the positron fraction. Indeed, the steepest allowed decline continues to be relatively slow, reaching the expected background flux only at energies beyond $E_{e^\pm} \sim 1$ TeV.

We see, then, that the primary results we have presented in this paper—that decaying DDM ensembles can successfully reproduce both AMS-02 and FERMI data and yield concrete predictions for the positron fraction at high energies—in most cases do not depend significantly on our choice of astrophysical approximations or computational tools. Indeed, as discussed in Sec. V, it is the relative softness of the $\Phi_{e^\pm}$ spectra from an entire decaying DDM ensemble which underlies these phenomenological successes, and this is an inherent property of the DDM framework which transcends the particular calculational procedures and astrophysical parameters chosen. Even in the most dramatic case in which we replace the MED propagation model with the rather extreme MIN propagation model, the very small remaining region of DDM parameter space continues to exhibit the "smoking gun" feature in which the positron fraction remains above background out to higher energies beyond those currently probed. Thus, while the specific quantitative results obtained using alternative approximations or computational tools may differ somewhat, this relative softness—which we have demonstrated contributes significantly to easing phenomenological tensions—is a real and direct consequence of the underlying particle physics of DDM ensembles.

Finally, before concluding, we emphasize that the criterion in Eq. (2.3) does not represent a constraint which our DDM framework must satisfy, but rather merely defines a phenomenologically interesting regime of parameter space within that framework. Indeed, regions of parameter space in which this criterion is not satisfied can also in principle yield models which reproduce AMS-02 positron-fraction data and at the same time satisfy other constraints on dark-matter decays. In general, such models lead to a more mundane set of predictions for the positron fraction at high energies, including the possibility of a relatively sharp downturn similar to that expected in traditional dark-matter models of the positron excess. Thus, while the observation of a slowly falling or relatively level positron excess in future AMS-02 data would strongly favor a decaying DDM ensemble over other possible dark-matter interpretations, the nonobservation of such a signal would not, in and of itself, rule out a DDM ensemble as an explanation of that excess.

VII. CONCLUSIONS

In this paper, we have examined the implications of cosmic-ray data—and, in particular, the recent AMS-02 measurement of the positron fraction—for models constructed within the Dynamical Dark Matter framework. Because the DDM framework generally includes dark-matter particles with lifetimes near the current age of the universe, present-day cosmic-ray data can be expected to have particular relevance for DDM. Our primary results can be summarized as follows:

(i) First, we have shown that DDM ensembles provide a viable dark-matter explanation of the existing positron excess. This is true even when the relevant astrophysical and cosmological constraints are taken into account. Indeed, as we have seen, the partitioning of the dark-matter abundance $\Omega_{\rm CDM}$ across an entire ensemble of dark-sector fields obeying certain scaling relations provides a natural and well-motivated method of softening the $e^{\pm}$ injection spectrum and reproducing the existing data. Moreover, for a DDM ensemble whose constituents decay primarily to $\mu^+\mu^-$, we have found that this softening alone is sufficient to obtain consistency with the positron fraction observed by AMS-02 and the combined $e^{\pm}$ flux observed by FERMI.

(ii) Second, we have shown that those DDM scenarios which successfully reproduce the observed positron excess generically predict that the positron fraction either levels off or falls gradually at higher energies beyond those currently probed. By contrast, conventional dark-matter scenarios for explaining the positron excess generically predict a very different behavior: an abrupt downturn in the positron fraction at higher energies. Thus, if we attribute the positron excess to dark-matter physics, we may interpret a relatively flat positron excess curve as a ''smoking gun'' of the DDM framework.

(iii) Finally, we note that in order to reproduce the positron-fraction curve observed by PAMELA and AMS-02, a traditional dark-matter candidate typically must be quite heavy, with a mass $m_\chi \gtrsim 1$ TeV. By contrast, we have shown that those DDM ensembles which accurately reproduce the observed positron-fraction curve generically tend to include large numbers of lighter constituent particles ϕ_n, with masses in the range $300\ \text{GeV} \lesssim m_n \lesssim 700\ \text{GeV}$. The presence of such lighter particles playing an active role in the dark sector opens up a broader variety of possibilities for detection using other, complementary probes of the dark sector—including colliders, direct-detection experiments, etc.

Moreover, as we have shown in Sec. VI, these results are largely independent of a variety of input assumptions associated with the nature of our DDM ensemble or the modeling of the external astrophysical environment.

Despite these results, it is important to stress that our analysis in this paper has been fundamentally predicated on an underlying dark-matter interpretation of the positron excess. However, there do exist alternative explanations of these cosmic-ray anomalies. Indeed, as has been shown in Refs. [17,57], a contribution to Φ_{e^+} and Φ_{e^-} from a population of nearby pulsars may provide an alternative explanation for the positron excess reported by PAMELA, FERMI, and other cosmic-ray experiments. This explanation is a compelling one because it offers an origin for this excess in terms of standard astrophysical processes rather than new physics. Moreover, the pulsar explanation is also of particular interest in relation to the cosmic-ray phenomenology of DDM ensembles. Indeed, much like the net contribution from a DDM ensemble, the net contribution to Φ_{e^+} and Φ_{e^-} from a population of nearby pulsars represents the sum over a large number of individual contributions. It is therefore reasonable to expect that many of the same characteristic features which arise in the Φ_{e^+} and Φ_{e^-} spectra associated with DDM ensembles should also appear within the range of possible spectra associated with specific pulsar populations. Indeed, the shape of the overall positron-fraction curve associated with a collection of pulsars may be difficult to distinguish from that associated with a DDM ensemble.

However, in general one can measure more than the mere *shape* of such a differential flux; one can also study the *directionality* associated with its individual angular contributions. Directionality is especially important in this situation because it provides a critical method of distinguishing the case of a DDM ensemble from that of a population of pulsars. In the pulsar case, an anisotropy is expected in the signal contributions as a function of energy due to the differing positions of the individual contributing pulsars. In fact, if a single nearby pulsar (or a small number thereof) is essentially responsible for the observed positron excess, this anisotropy should be observable over a wide range of energies $E_{e^\pm}$ at the Cherenkov Telescope Array (CTA) [58]. By contrast, it is reasonable to imagine that the constituent particles within a DDM ensemble are distributed in roughly the same manner throughout the galactic halo, and thus no significant flux anisotropy is to be expected (other than a slight overall flux enhancement in the direction of the galactic center, an enhancement which is unlikely to be detected at future experiments).

Provided that the contributions of individual pulsars can be resolved, we conclude that forthcoming data on the anisotropy of the observed positron flux may play an important role in differentiating between a collection of local pulsars and a DDM ensemble as explanations for the observed positron excess. However, we note that the propagation of cosmic rays in the local environment is

very complicated, and it may ultimately be very difficult to draw any firm conclusions in the case that no anistropy is ultimately detected. These issues are discussed more fully in Ref. [59]. Likewise, we note that there also exist even more prosaic models that can potentially explain the positron excess. These include, for example, models [60] in which the excess positrons are generated as secondary products of hadronic interactions inside natural cosmic-ray sources, such as supernova remnants, and are thus naturally accelerated in a way that endows them with a relatively flat spectrum. Measurements of the secondary nuclei produced by cosmic-ray spallation could potentially be used in order to discriminate between these possibilities [61].

ACKNOWLEDGMENTS

We would like to thank V. Bindi, D. Hooper, I. Low, D. Marfatia, P. Sandick, J. Siegal-Gaskins, and X. Tata for discussions. K. R. D. is supported in part by the Department of Energy under Grants No. DE-FG02-04ER-41298 and No. DE-FG02-13ER-41976, and in part by the National Science Foundation through its employee IR/D program. J. K. is supported in part by DOE Grants No. DE-FG02-04ER-41291 and No. DE-FG02-13ER-41913. B. T. is supported in part by DOE Grant No. DE-FG02-04ER-41291. The opinions and conclusions expressed herein are those of the authors, and do not represent either the Department of Energy or the National Science Foundation.

[1] M. Aguilar *et al.* (AMS Collaboration), Phys. Rev. Lett. **110**, 141102 (2013).
[2] S. W. Barwick *et al.* (HEAT Collaboration), Astrophys. J. **482**, L191 (1997).
[3] M. Aguilar *et al.* (AMS Collaboration), Phys. Rep. **366**, 331 (2002); **380**, 97(E) (2003).
[4] M. Aguilar *et al.* (AMS-01 Collaboration), Phys. Lett. B **646**, 145 (2007).
[5] O. Adriani *et al.* (PAMELA Collaboration), Nature (London) **458**, 607 (2009).
[6] O. Adriani, G. C. Barbarino, G. A. Bazilevskaya, R. Bellotti, M. Boezio, E. A. Bogomolov, L. Bonechi, M. Bongi, V. Bonvicini, and S. Borisov, Astropart. Phys. **34**, 1 (2010).
[7] M. Ackermann *et al.* (Fermi LAT Collaboration), Phys. Rev. Lett. **108**, 011103 (2012).
[8] O. Adriani *et al.* (PAMELA Collaboration), Phys. Rev. Lett. **105**, 121101 (2010).
[9] A. A. Abdo *et al.* (Fermi LAT Collaboration), Phys. Rev. Lett. **102**, 181101 (2009); M. Ackermann *et al.* (Fermi LAT Collaboration), Phys. Rev. D **82**, 092004 (2010).
[10] A. A. Abdo *et al.* (Fermi-LAT Collaboration), Phys. Rev. Lett. **104**, 101101 (2010).
[11] T. E. Montroy, P. A. R. Ade, J. J. Bock, J. R. Bond, J. Borrill, A. Boscaleri, P. Cabella, C. R. Contaldi *et al.*, Astrophys. J. **647**, 813 (2006).
[12] C. L. Reichardt, P. A. R. Ade, J. J. Bock, J. R. Bond, J. A. Brevik, C. R. Contaldi, M. D.Daub, J. T. Dempsey *et al.*, Astrophys. J. **694**, 1200 (2009).
[13] E. Komatsu *et al.* (WMAP Collaboration), Astrophys. J. Suppl. Ser. **180**, 330 (2009).
[14] P. A. R. Ade *et al.* (Planck Collaboration), arXiv:1303.5076.
[15] L. Bergstrom, T. Bringmann, and J. Edsjo, Phys. Rev. D **78**, 103520 (2008); M. Cirelli and A. Strumia, Proc. Sci., IDM 2008 (2008) 089; I. Cholis, L. Goodenough, D. Hooper, M. Simet, and N. Weiner, Phys. Rev. D **80**, 123511 (2009); V. Barger, W. Y. Keung, D. Marfatia, and G. Shaughnessy, Phys. Lett. B **672**, 141 (2009); M. Cirelli, M. Kadastik, M. Raidal, and A. Strumia, Nucl. Phys. B813, 1 (2009); A. E. Nelson and C. Spitzer, J. High Energy Phys. 10 (2010) 066; N. Arkani-Hamed, D. P. Finkbeiner, T. R.Slatyer, and N. Weiner, Phys. Rev. D **79**, 015014 (2009); I. Cholis, D. P. Finkbeiner, L. Goodenough, and N. Weiner, J. Cosmol. Astropart. Phys. 12 (2009) 007; Y. Nomura and J. Thaler, Phys. Rev. D **79**, 075008 (2009); P.-f. Yin, Q. Yuan, J. Liu, J. Zhang, X.-j. Bi, and S.-h. Zhu, Phys. Rev. D **79**, 023512 (2009); R. Harnik and G. D. Kribs, Phys. Rev. D **79**, 095007 (2009); P. J. Fox and E. Poppitz, Phys. Rev. D **79**, 083528 (2009); M. Pospelov and A. Ritz, Phys. Lett. B **671**, 391 (2009); K. M. Zurek, Phys. Rev. D **79**, 115002 (2009); J. D. March-Russell and S. M. West, Phys. Lett. B **676**, 133 (2009); P. Grajek, G. Kane, D. Phalen, A. Pierce, and S. Watson, Phys. Rev. D **79**, 043506 (2009); S. Chang and L. Goodenough, Phys. Rev. D **84**, 023524 (2011).
[16] L. Feng, R.-Z. Yang, H.-N. He, T.-K. Dong, Y.-Z. Fan, and J. Chang, arXiv:1303.0530 [Phys. Rev. D (to be published)]; A. De Simone, A. Riotto, and W. Xue, J. Cosmol. Astropart. Phys. 05 (2013) 003; 05 (2013) 003; Q. Yuan, X.-J. Bi, G.-M. Chen, Y.-Q. Guo, S.-J. Lin, and X. Zhang, arXiv:1304.1482; M. Ibe, S. Iwamoto, S. Matsumoto, T. Moroi, and N. Yokozaki, J. High Energy Phys. 08 (2013) 029 ; H.-B. Jin, Y.-L. Wu, and Y.-F. Zhou, arXiv:1304.1997; Y. Kajiyama, H. Okada, and T. Toma, arXiv:1304.2680; L. Feng and Z. Kang, arXiv:1304.7492; L. Bergstrom, T. Bringmann, I. Cholis, D. Hooper, and C. Weniger, Phys. Rev. Lett. **111**, 171101 (2013); K. Kohri and N. Sahu, arXiv:1306.5629 [Phys. Rev. D (to be published)].
[17] I. Cholis and D. Hooper, Phys. Rev. D **88**, 023013 (2013).
[18] A. Ibarra, A. Ringwald, D. Tran, and C. Weniger, J. Cosmol. Astropart. Phys. 08 (2009) 017.
[19] H.-C. Cheng, W.-C. Huang, I. Low, and G. Shaughnessy, J. Cosmol. Astropart. Phys. 01 (2013) 033.
[20] V. Barger, Y. Gao, W. Y. Keung, and D. Marfatia, Phys. Rev. D **80**, 063537 (2009).
[21] M. Ibe, S. Matsumoto, S. Shirai, and T. T. Yanagida, J. High Energy Phys. 07 (2013) 063.

[22] K. R. Dienes and B. Thomas, Phys. Rev. D **85**, 083523 (2012).
[23] K. R. Dienes and B. Thomas, Phys. Rev. D **85**, 083524 (2012).
[24] K. R. Dienes and B. Thomas, Phys. Rev. D **86**, 055013 (2012).
[25] K. R. Dienes, S. Su, and B. Thomas, Phys. Rev. D **86**, 054008 (2012).
[26] K. R. Dienes, J. Kumar, and B. Thomas, Phys. Rev. D **86**, 055016 (2012).
[27] A. Arvanitaki, S. Dimopoulos, S. Dubovsky, N. Kaloper, and J. March-Russell, Phys. Rev. D **81**, 123530 (2010).
[28] D. Chialva, P. S. B. Dev, and A. Mazumdar, Phys. Rev. D **87**, 063522 (2013).
[29] J. F. Navarro, C. S. Frenk, and S. D. M. White, Astrophys. J. **462**, 563 (1996).
[30] A. Ibarra and D. Tran, J. Cosmol. Astropart. Phys. 07 (2008) 002.
[31] M. Cirelli, G. Corcella, A. Hektor, G. Hütsi, M. Kadastik, P. Panci, M. Raidal, F. Sala, and A. Strumia, J. Cosmol. Astropart. Phys. 03 (2011) 051; 10 (2012) E01.
[32] T. Delahaye, R. Lineros, F. Donato, N. Fornengo, and P. Salati, Phys. Rev. D **77**, 063527 (2008).
[33] F. Donato, N. Fornengo, D. Maurin, and P. Salati, Phys. Rev. D **69**, 063501 (2004).
[34] A. Ibarra, D. Tran, and C. Weniger, J. Cosmol. Astropart. Phys. 01 (2010) 009.
[35] D. Grasso *et al.* (FERMI-LAT Collaboration), Astropart. Phys. **32**, 140 (2009).
[36] D. Gaggero and L. Maccione, arXiv:1307.0271.
[37] L. J. Gleeson and W. I. Axford, Astrophys. J. **154**, 1011 (1968).
[38] J. S. Perko, Astron. Astrophys. **184**, 119 (1987).
[39] L. Maccione, Phys. Rev. Lett. **110**, 081101 (2013).
[40] L. Zhang, J. Redondo, and G. Sigl, J. Cosmol. Astropart. Phys. 09 (2009) 012.
[41] M. Cirelli, P. Panci, and P. D. Serpico, Nucl. Phys. **B840**, 284 (2010).
[42] M. Cirelli, E. Moulin, P. Panci, P. D.Serpico, and A. Viana, Phys. Rev. D **86**, 083506 (2012).
[43] Fermi-LAT Collaboration, Astrophys. J. **720**, 435 (2010); K. N. Abazajian, S. Blanchet, and J. P. Harding, Phys. Rev. D **84**, 103007 (2011); F. W. Stecker and T. M. Venters, Astrophys. J. **736**, 40 (2011); B. D. Fields, V. Pavlidou, and T. Prodanovic, Astrophys. J. **722**, L199 (2010); C.-A. Faucher-Giguere and A. Loeb, J. Cosmol. Astropart. Phys. 01 (2010) 005; B. S. Hensley, V. Pavlidou, and J. M. Siegal-Gaskins, Mon. Not. R. Astron. Soc. **433**, 591 (2013).
[44] M. Papucci and A. Strumia, J. Cosmol. Astropart. Phys. 03 (2010) 014; L. Zhang, C. Weniger, L. Maccione, J. Redondo, and G. Sigl, J. Cosmol. Astropart. Phys. 06 (2010) 027.
[45] G. Bertone, G. Sigl, and J. Silk, Mon. Not. R. Astron. Soc. **326**, 799 (2001); **337**, 98 (2002); D. P. Finkbeiner, arXiv: astro-ph/0409027; D. Hooper, Phys. Rev. D **77**, 123523 (2008).
[46] K. Ishiwata, S. Matsumoto, and T. Moroi, Phys. Rev. D **79**, 043527 (2009).
[47] X.-L. Chen and M. Kamionkowski, Phys. Rev. D **70**, 043502 (2004).
[48] N. Padmanabhan and D. P. Finkbeiner, Phys. Rev. D **72**, 023508 (2005).
[49] S. Galli, F. Iocco, G. Bertone, and A. Melchiorri, Phys. Rev. D **80**, 023505 (2009).
[50] T. R. Slatyer, N. Padmanabhan, and D. P. Finkbeiner, Phys. Rev. D **80**, 043526 (2009).
[51] D. P. Finkbeiner, L. Goodenough, T. R. Slatyer, M. Vogelsberger, and N. Weiner, J. Cosmol. Astropart. Phys. 05 (2011) 002.
[52] T. R. Slatyer, Phys. Rev. D **87**, 123513 (2013).
[53] S. Torii *et al.* (PPB-BETS Collaboration), arXiv:0809.0760.
[54] J. Chang *et al.*, Nature (London) **456**, 362 (2008).
[55] F. Aharonian *et al.* (H.E.S.S. Collaboration), Astron. Astrophys. **508**, 561 (2009).
[56] K. G. Begeman, A. H. Broeils, and R. H. Sanders, Mon. Not. R. Astron. Soc. **249**, 523 (1991).
[57] D. Hooper, P. Blasi, and P. D. Serpico, J. Cosmol. Astropart. Phys. 01 (2009) 025; L. Maccione, Phys. Rev. Lett. **110**, 081101 (2013); P.-F. Yin, Z.-H. Yu, Q. Yuan, and X.-J. Bi, Phys. Rev. D **88**, 023001 (2013); D. Gaggero, L. Maccione, G. Di Bernardo, C. Evoli, and D. Grasso, Phys. Rev. Lett. **111**, 021102 (2013).
[58] T. Linden and S. Profumo, Astrophys. J. **772**, 18 (2013).
[59] E. Borriello, L. Maccione, and A. Cuoco, Astropart. Phys. **35**, 537 (2012); M. D. Kistler, H. Yuksel, and A. Friedland, arXiv:1210.8180 [Phys. Rev. Lett. (to be published)].
[60] P. Blasi, Phys. Rev. Lett. **103**, 051104 (2009).
[61] P. Mertsch and S. Sarkar, Phys. Rev. Lett. **103**, 081104 (2009).